Development and Validation of a Paralimbic Related Subcortical Brain Dysmaturation MRI Score in Infants with Congenital Heart Disease

William T. Reynolds, BS*[1], Jodie K. Votava-Smith, MD*[2], George Gabriel, PhD*[4], Vince Lee, BS[5], Vidya Rajagopalan, PhD[2], Yijen Wu, PhD[4], XiaoQin Liu[4], MD, Hisato Yagi, PhD[4], Ruby Slabicki, BA[5], Brian Gibbs, PhD,[4] Nhu N. Tran, PhD[3], Molly Weisert, MD[2], Laura Cabral PhD[5], Subramanian Subramanian, M.D[5], Julia Wallace, BA[5], Sylvia del Castillo, MD[6], Tracy Baust, BA[7], Jacqueline Weinberg, MD[8], Lauren Lorenzi Quigley, PhD[10], Jenna Gaesser MD[9], Sharon H. O'Neil PhD[11], Vanessa Schmithorst PhD[5], Rafael Ceschin, PhD**[5] Cecilia Lo, PhD**[4], and Ashok Panigrahy, MD**[5]

1. Department of Biomedical Informatics, University of Pittsburgh School of Medicine, Pittsburgh, PA
2. Department of Pediatrics, Division of Cardiology, Children's Hospital Los Angeles, and Keck School of Medicine, University of Southern California, Los Angeles, CA
3. Fetal and Neonatal Institute, Division of Neonatology Children's Hospital Los Angeles, Department of Pediatrics, Keck School of Medicine, University of Southern California, Los Angeles, CA
4. Department of Developmental Biology, University of Pittsburgh School of Medicine, Pittsburgh, PA
5. Department of Pediatric Radiology, Children's Hospital of Pittsburgh of UPMC and University of Pittsburgh School of Medicine, Pittsburgh, PA
6. Department of Anesthesiology, Critical Care Medicine Children's Hospital Los Angeles, Los Angeles, CA
7. Department of Critical Care Medicine, University of Pittsburgh, Pittsburgh, PA
8. Department of Cardiology, University of Pittsburgh School of Medicine, Pittsburgh, PA
9. Department of Neurology and Child Development, University of Pittsburgh School of Medicine, Pittsburgh, PA
10. Cardiac Neurodevelopmental Care Program, Children's Hospital of Pittsburgh of UPMC, Pittsburgh, PA
11. Division of Neurology and The Saban Research Institute, Children's Hospital Los Angeles, Department of Pediatrics, Keck School of Medicine, University of Southern California, Los Angeles, CA

*co-first authors; **co-senior authors

Short Title: Subcortical paralimbic abnormalities and outcomes in infant and CHD mouse model

Address Correspondence and Reprint Request to:
Ashok Panigrahy, MD
Department of Pediatric Radiology
Children's Hospital of Pittsburgh of UPMC
4401 Penn Avenue
Pittsburgh, PA 15224
Tel: 412-692-5510
Fax: 412-864-8622
apanigrahyranjan@gmail.com

Abstract

Background

Brain magnetic resonance imaging (MRI) of infants with congenital heart disease (CHD) shows brain immaturity assessed via a cortical-based semi-quantitative score. Our primary aim was to develop an infant paralimbic-related subcortical-based semi-quantitative dysmaturation score, a brain dysplasia score (BDS), to detect abnormalities in CHD infants and predict clinical outcomes. Our secondary aim was to validate our BDS in a preclinical mouse model of hypoplastic left heart syndrome.

Methods

A paralimbic-related subcortical BDS, derived from structural MRIs of infants with CHD, was correlated with clinical risk factors, regional cerebral volumes, feeding and 18-month neurodevelopmental outcomes. The BDS was validated in a known CHD mouse model named *Ohia* with two disease-causing genes, *Sap130* and *Pchda9*. To relate clinical findings, RNA-Seq was completed on *Ohia* animals.

Findings

BDS showed high incidence of paralimbic-related subcortical abnormalities (including olfactory, cerebellar, and hippocampal abnormalities) in CHD infants (n=215) compared to healthy controls (n=92). BDS correlated with reduced cortical maturation, developmental delay, poor language and feeding outcomes, and increased length of stay. *Ohia* animals (n=63) showed similar BDS findings, and RNA-Seq analysis showed altered neurodevelopmental and feeding pathways. *Sap130* mutants correlated with a more severe BDS whereas *Pcdha9* correlated with a milder phenotype.

Interpretation

Our BDS is sensitive to dysmaturational differences between CHD and healthy controls, and predictive of poor outcomes. A similar spectrum of paralimbic-related subcortical abnormalities exists between human and *Ohia* mutants suggesting a common genetic mechanistic etiology.

Funding

National Library of Medicine, Department of Defense, National Heart, Lung, and Blood Institute, National Institute on Aging, Southern California Clinical and Translational Sciences Institute, Additional Ventures Foundation, Saban Research Institute, Children's Hospital Los Angeles Clinical Services Research Grant, and National Institute of Nursing Research. Funding award numbers can be found in the acknowledgment section.

Non-standard Abbreviations and Acronyms

ECM: Episcopic Confocal Microscopy, CHD: congenital heart disease, HLHS: hypoplastic left heart syndrome, MRI: magnetic resonance imaging, , WMI: white matter injury, GA: gestational age, PCA: post-conceptional age, BDS: brain dysplasia score.

Keywords

Olfactory Bulb, Hippocampus, Cerebellum, Feeding Outcome, Neurodevelopmental Outcome, Ohia HLHS Mouse Mutants

Research In Context

Evidence before

The number of clinical and research MRI studies in neonatal/infant CHD subjects has increased dramatically in the last two decades. Previous studies have developed brain MRI scores that have focused on cortical structural maturation and acquired brain injury. Paralimbic-related subcortical regions are important for the development of cognitive and visuomotor functions in early development. Levering a large infant brain MRI dataset and a large-scale genetic mouse screen, we theorized that a paralimbic-related subcortical brain MRI score could assist clinicians with outcome prediction in CHD infants.

Added Value

This work aims to develop a subcortical morphological scoring system that could be applied to either clinical or research MRI scans and could improve the ability of clinicians and neuroradiologists to predict not only those at risk for suboptimal neurodevelopmental outcomes but also associated co-morbidities. We discovered not only are there paralimbic-related subcortical structural abnormalities that a brain MRI score can detect but also that this score predicted poor language outcomes, poor feeding outcomes, and increased post-surgical length of stay. We also found that the genetic model of hypoplastic left heart syndrome, the most severe form of CHD, also demonstrated a similar pattern of paralimbic related subcortical brain abnormalities.

Implications

This novel scoring system developed by our group has implications for early detection of at-risk CHD individuals for poor outcomes, both neurodevelopmental and quality of life. This subcortical paralimbic brain dysplasia score is a simple tool that can be easily added to neuroradiological workflows that can lead to better outcome prediction for children with CHD. Our scoring system helps us to better serve our population, allowing clinicians and researchers to prognosticate highest risk individuals who will benefit from the earliest forms of intervention.

Introduction

Congenital heart disease (CHD) affects 1% of live births each year.[1,2] As the surgical care for CHD improves, there remains lingering increased risk of poor neurodevelopmental outcomes for patients with CHD across the lifespan. The mechanism for neurodevelopmental disabilities in non-syndromic CHD is unknown and is thought to be related to fetal exposure to reduced substrate delivery/hypoxia or a genetic underpinning. Genetic abnormalities are detected in approximately 50% of children with syndromic CHD, and in approximately 10% of children without a recognizable clinical phenotype.[3] Significant overlap is present between deleterious de novo mutations and previously reported mutations associated with neurodevelopmental disorders,[4] suggesting that genetic mutations that cause CHD, may also be important in the etiology of neurodevelopmental deficits.[5,6] Smaller brain volumes and dysmature brain structures are seen in neonates and fetuses with CHD before cardiac surgery, suggesting that innate and/or prenatal factors may play an important role in altering brain development.[7-9] Within our current understanding of neurogenesis, there is little known about the role that deep grey and subcortical regions play in mediating poor neurodevelopmental outcomes in relation to genetic alterations. Recent animal models and correlative neuropathological studies suggest that cortical dysmaturation is linked to white matter abnormalities, including developmental vulnerability of the subplate in CHD.[10,11] Recent neuroimaging studies have documented paralimbic related subcortical morphological abnormalities in CHD patients across the lifespan,[12-16] but the relationship between paralimbic-related subcortical morphological abnormalities and clinical and neurodevelopmental outcomes in CHD is also unknown.[17-20]

Children with CHD are at a higher risk of developing brain dysmaturation, a generalized term encompassing abnormal and delayed development of brain macro- and microstructure[21-25]. CHD patients are also at risk for acquired brain injury, including infarcts and small vessel disease across lifespan as detected by conventional neuroimaging studies. Clinical neuroimaging studies are also becoming more common to obtain in patients during the peri-operative period based on recently published guidelines. Most conventional semi-quantitative MRI scoring systems in CHD patients have exclusively focused on either acquired brain injury or cortical maturation assessment, particularly in the neonatal period.[26-33] We recently developed and validated an infant semi-quantitative score that extending beyond cortical maturation and acquired brain injury to include morphological alterations in paralimbic-related subcortical structures (including cerebellum, hippocampus, olfactory bulb abnormalities), CSF-related abnormalities (including increased extra-axial CSF in frontotemporal regions) and the corpus callosum known as a brain dysplasia score (BDS), informed by preclinical models of CHD, specifically hypoplastic left heart syndrome (HLHS). We focused our analysis on paralimbic-related subcortical structures that are known to undergo neurogenesis in early development and across the lifespan, including the olfactory bulbs, hippocampus, and cerebellum. We have recently described a similar pattern of structural subcortical dysmaturation both in human infants with CHD and genetically relevant ciliary motion dysfunction, and also in relation to preclinical models of CHD including hypoplastic left heart syndrome (HLHS).[34-40] We have previously shown that the BDS correlates with abnormal neonatal brain white matter connectivity patterns[41] but have yet to validate this scoring system in a large dataset in relation to clinical and neurodevelopmental outcomes. Here, we used quantitative structural brain magnetic resonance imaging (MRI) in infants with CHD to test the hypothesis that subcortical morphological measurements could be assessed using a qualitative scoring system termed brain dysplasia score (BDS) and that these subcortical structures are potential predictors of not only infant cortical maturation and regional brain volumes but also are predictors of poor clinical and neurodevelopmental outcomes.[12-15,21,42,43]

To further validate our subcortical BDS from a genetic perspective, we leveraged the *Ohia* mouse model of HLHS recovered from a large-scale mouse mutagenesis screen. In *Ohia* mice with HLHS, phenotypic mutations primarily arise from homozygous mutations in two genes, a chromatin modifying protein Sin3A-associated protein 130 (*Sap130*), and protocadherin A9 (*Pcdha9*), a cell adhesion protein in the a-protocadherin gene cluster.[44] Importantly, both genes are known to have important roles in brain health-related outcomes. For example, the clustered protocadherins provide cell surface diversity by encoding unique neuronal identity essential for patterning synaptic connectivity.[45] Mice with PCDHA mutations have deficiencies in both brain connectivity and neurobehavioral deficits.[46] Moreover, mutations in both PCDHA and SIN3A are associated with autism and Rett Syndrome in humans.[47-49] Importantly, the SIN3A complex also contains transcription factors known to regulate developmental and lifespan neurogenesis.[50,51] Given the prominent roles of PCDHA and SIN3A in human neurogenesis and brain development, we used the *Ohia* mouse model for further validation of the hypothesis that the subcortical BDS could be used as a proxy of subcortical morphological and connectivity quantitative measurements and predict clinical and neurodevelopmental outcomes in human CHD infants.

Methods

Ethics

The study was HIPAA compliant and approved by the institutional review board (IRB) of Children's Hospital Los Angeles (CHLA) and Children's Hospital of Pittsburgh (CHP) of the University of Pittsburgh Medical Center (UPMC) and written informed consent was obtained from each subject, except for a few patients in which MRI was obtained clinically, and retrospective use of the data was approved by the IRB protocol (CHLA-CCI-09-00055, CCI-10-00235, University of Pittsburgh- 20030213,19100215, 19030204). All experiments were performed per the institutional guidelines and regulations.

Patient Recruitment and Clinical Data Collection

This study is a secondary analysis of neonates with CHD (term and preterm) undergoing brain MRI scans who were recruited as part of a prospective, observational study from two large medical centers, CHLA and CHP. Neonatal CHD cases were prospectively recruited from (1) pregnancies with fetal CHD confirmed with fetal echocardiography and (2) postnatal admissions to the cardiothoracic intensive care unit postoperatively between 2002-2016 and (3) infants with both preterm and term CHD undergoing clinically indicated brain MRI scans at approximately term-equivalent gestational age (GA) were recruited both prospectively and retrospectively in the peri-operative period from 2002-2017. The inclusion criterion was critical CHD defined as a heart defect expected to require corrective or palliative cardiac surgery during infancy. Exclusion criteria for the CHD included documented major chromosomal abnormalities and major congenital brain malformations. Normal referents were recruited (1) from healthy pregnant volunteers and (2) postnatally from a normal newborn nursery. An additional comparison group was included which was comprised of preterm infants without CHD who were recruited from a high-risk NICU at the same institutions as previously published.[20,52-54] Details about the recruitment strategies have been described in multiple previous publications.[12,34,35,55-63]

There were 423 subjects that met the inclusion criteria for this study: 307 full term neonates (215 with CHD and 92 term controls) and 116 preterm neonates (65 with CHD born 25-36 weeks GA, and 51 preterm control patients born 24 – 36 weeks GA) (Figure 1). This is the dataset for which we performed the primary analysis of calculating a BDS and comparing the difference between groups.

Research Scans

Brain MRIs for CHD infants were obtained in either the preoperative (usually between 1-7 days) or postoperative period (up to 13 weeks postnatally, but often sooner). The age range for healthy controls ranged between birth and thirteen weeks postnatally, encompassing the same range of the CHD infants. Preoperative research brain imaging was conducted when on CHD subjects when the cardiothoracic intensive care unit (CTICU) team/cardiology team determined the patient was stable for transport to the MRI scanner. Postoperative research scan was performed at less than three months of postnatal age either as an inpatient or outpatient. Most of our scans were research indicated and as such no additional sedation/anesthesia was given for the scan purpose. Most of the pre-operative scans were performed on non-intubated non-sedated patients; however, if the patient was intubated and sedated for clinical reasons at the time of the scan, their clinically indicated sedation continued under care of the primary CTICU. team. The post-operative scans were performed when the infant was clinically stable and thus were done as "feed and bundle" scans without sedation. To minimize movement during imaging, infants were secured in Med-Vac Immobilization Bag (CFI Medical) with multiple levels of ear protection, including ear plugs, MiniMuffs (Natus Medical Incorporated), and standard headphones.

Clinical Scans

Patients in the clinically indicated brain MRI group were scanned at approximately term-equivalent GA either in the pre- or post-operative period as previously published.[58] The post-operative scan for both preterm CHD and term CHD groups was performed at least within 52 weeks corrected postconceptional age.

Neonatal Brain MRI Protocol

MRI studies were acquired: (1) GE 1.5T (Signa LX, GE Healthcare, Milwaukee, WI) MR system using a custom-built neonatal transmit-receive head coil, (2) Philips 3T Achieva MR System (Ver. 3.2.1.1) using standard 8-

channel SENSE head coil; and (3) Siemens Skyra 3T scanner using a 20-channel coil. Conventional imaging studies were acquired with the MRS studies and included a 3D coronal SPGR sequence (TE= 6 ms; TR=25 ms, FOV=18 cm; matrix=256 × 160; slice thickness 1.5 mm, spacing 0 mm) or axial and sagittal T1-weighted FLAIR sequences (TE=7.4, TR=2100; TI=750; FOV=20 cm; Matrix=256 × 160), axial T2-weighted FSE sequence (TE=85ms, TR=5000ms, FOV=20 cm, matrix =320 × 160 or 256 × 128) and a diffusion-weighted sequence (TE=80; TR=10000; FOV=22 cm; Matrix = 128 × 128; slice thickness =4.5 mm, spacing 0 mm). The 3D T1-weighted, T2-weighted, and diffusion-weighted images were reviewed by two pediatric neuroradiologists for evidence of punctate white matter lesion, hypoxic-ischemic injury, acute focal infarction, and hemorrhage as previously described and were used to construct dichotomized and composite brain injury scores.[64]

Subcortical brain dysplasia MRI score (BDS) derivation

Our development of the subcortical based BDS has been derived from observations from both preclinical mouse CHD mutants and human CHD infants from recent studies from our group.[21,22,36,39,65-67] The evaluation for brain dysplasia in our human CHD population is conducted by examining the following structures: cerebellar hemispheres (both left and right together), cerebellar vermis, right olfactory bulb, right olfactory sulcus, left olfactory bulb, left olfactory sulcus, hippocampus, choroid plexus, brain stem, corpus callosum, and supratentorial extra-axial fluid. Supplemental Figure 1 depicts a visualization of how the BDS was calculated. Except for the supratentorial extra-axial fluid, each of the structures listed were evaluated on whether they appear normal or abnormal. For cerebellar hemispheres and cerebellar vermis, they were scored for hypoplasia (small volume) and dysplasia (abnormal shape). Likewise, the olfactory bulbs and sulci were evaluated as separate structures for purposes of scoring. Based on the finding, a binary number score is given for each structure, with a score of 0 assigned for normal and a score of 1 for abnormal. For olfactory bulbs and sulci, both hypoplastic and absent findings are treated as abnormal and given a score of 1. For supratentorial extra-axial fluid, the structural features demonstrate different gradations of abnormality – none, mild, moderate, or severe fluid accumulation – and thus successively higher integer scores are assigned as the severity of abnormality becomes greater. The integer scores for each of the structures were then summed to create the BDS with "olfactory correction" which treats both absent and hypoplastic olfactory abnormalities as one score point, thus making the weighting of the olfactory system in line with cerebellum and hippocampus. Higher BDS values can be thought of as having a "worse" score as subjects had more abnormalities present. A subset of cases was reviewed by two raters to validate the scoring.

Similar to our BDS, a brain injury score was calculated for each human subject. The composite brain injury score consisted of four criteria with each criterion being scored as a 1 if present in the subject. The four criteria were hemorrhage, infarct, hypoxic ischemic injury, and periventricular white matter injury (PWMI). A dichotomized version was also calculated for each individual and was scored as a 1 or 0. If the original brain injury score was greater than 0, then the composite score was a 1; otherwise, the score was a 0. A visual depiction of the brain injury scores can be found in Supplemental Figure 2.

Structural Co-variate Analysis: Cortical Maturation Score and Regional Brain Volumetric Analysis

We correlated BDS with a classic cortical Total Maturation Score (TMS) and regional brain volumes. A cortical TMS was calculated for all subjects with brain MRI included in this analysis. A subset of the full cohort (term controls and CHD scanned at 3T imaging, n=105) underwent cerebral regional volumetric segmentation for structural co-variate analysis. To determine the relationship between our qualitative BDS and quantitative regional morphological dysmaturation, we performed regional brain morphometric techniques including volumetric segmentation of total intracranial cerebral spinal fluid (CSF), cortical grey matter, cortical white matter, deep grey nuclei, brainstem, and cerebellum using a neonatal and infant brain segmentation age-specific atlas. We further segmented total intracranial CSF into three compartments: supratentorial extra-axial CSF, infratentorial extra-axial CSF and intraventricular CSF. Our group used the above age-specific atlas to build a semi-automated brain parcellation pipeline for use in neonates and young infants (Supplemental Figure 3). The automated processing pipeline which was previously described in by our group,[35] was developed using Nipype and interfaces with several image registration algorithms using age-appropriate neonatal/infant templates to accommodate different post-conceptional ages in the patient cohort. Our methodology for volumetric segmentation of neonatal brain has been previously described.[68,69] We further refined this methodology for the current study because of the wide range of post-conceptional ages of neuroimaging studies and the resulting need to use a range of neonatal and infant age-appropriate templates. We also performed validation experiments to ensure optimal performance with this

neonatal/infant CHD cohort with mild brain dysplasia. We processed each patient's T1 and T2 volumetric images in parallel to optimize registration parameters uniquely to each tissue contrast. First, the images were cropped, and brain extracted using FSL BET. The volumetric images (T1 and T2 separately) were then biasfield corrected using FSL's FAST segmentation. We then registered the bias-field corrected images to the tissue contrast specific and post-conceptional age matched template, created by Serag et. al,[70] using a non-linear registration from Advanced Normalization Tools (ANTs). The output transformations were inversed and applied to the template space tissue probability maps provided with the neonatal atlas. This transformation results in subject-space tissue probability maps. We calculated tissue volumes by thresholding the partial volume maps at a visually acceptable lower bound and extracting the volume from the binarized mask. The subject-space segmentations were manually checked for accuracy by an expert pediatric neuroradiologist (AP) blinded to patient diagnosis.

Clinical Risk Factor Analysis

We correlated BDS with clinical risk factors. Analysis of clinical risk factors included a subset of subjects with critical CHD who required corrective or palliative cardiac surgery within the first month of life who were prospectively enrolled for pre and postoperative brain MRI scans from 2009-2016. Two hundred ninety-one subjects were prospectively enrolled from June 2009 to October 2016. Of these subjects, 158 met exclusion criteria including 57 with no MRI done, 38 due to prematurity, 38 passed the age threshold, 11 expired preoperatively, 10 had no neonatal surgery and 4 had a postnatal major genetic diagnosis. Of the 133 term CHD infants with brain MRI meeting inclusion criteria, 90 subjects had sufficient imaging quality for structural analysis and clinical risk factor data collected. comprised the study group for this analysis. Subjects that had a known major chromosomal abnormality, were premature (<=36 weeks of age), died prior to MRI or did not require neonatal cardiac surgery were excluded in this analysis. Clinical data was collected from the electronic medical records and included 18 patient-specific and 9 preoperative variables associated with preoperative scan and 6 intra-operative (e.g., cardiopulmonary bypass, deep hypothermic circulatory arrest times) and 12 postoperative variables associated with postoperative scan, as described previously.[59,71] CHD lesions were classified in several ways (not mutually exclusive) including postnatal cyanosis, presence of aortic arch obstruction, single vs. double ventricles, d-transposition of the great arteries, conotruncal defects, heterotaxy, whether the lesion alters fetal cerebral substrate delivery and severity of this alteration (normal, altered, severely altered).

Feeding Outcomes

We correlated the BDS with feeding outcomes. The feeding outcome study group consisted of term infants with CHD who had neonatal brain MRI with brain dysplasia score between 2003-2015, enrolled both prospectively for research MRI and retrospectively after clinical MRI, at CHLA and CHP. Subjects with major gastrointestinal anomalies or surgeries, a diagnosis of CHARGE syndrome, death within the first 30 days of life, or death prior to initiation of feeds were excluded from the feeding analysis. For the feeding study, we evaluated 177 term infants with CHD who had MRI that were used to calculate BDS as described above. Of those, 32 were excluded including 14 with major gastrointestinal anomalies or surgeries, 1 with brain anomaly, 6 with CHARGE syndrome, and 11 that died in the first 30 days or prior to initiation of feeds. Therefore, the feeding analysis group consisted of 145 subjects of which 81 were from CHLA and 64 from CHP. The inpatient medical records were assessed for the following feeding-related variables: presence of dysphagia, aspiration, gastroesophageal reflux, gastrointestinal dysmotility, intestinal malrotation, vocal cord paralysis, use of enteral tube feeding (including nasogastric, nasojejunal, or surgically placed gastric or jejunal tubes), lack of oral feeding prior to neonatal hospital discharge, and length of neonatal hospitalization.

Neurodevelopmental Outcomes

For neurodevelopmental outcomes assessment, Bayley Scales of Infant and Toddler Development or Battelle Developmental Inventory were completed by a licensed psychologist in a subset of patients. A total of 90 subjects (CHLA n=32, CHP n=58) had early neurodevelopmental outcome data obtained between 15 to 18 months postnatal age. The standard score for each developmental domain (motor, language/communication, cognitive, and social/emotional) was evaluated. Developmental delay was defined as a standard score greater than 2 standard deviations below the mean in 1 developmental domain. Global developmental delay was defined as a standard score greater than 2 standard deviations below the mean in 2 or more developmental domains. The following criteria was used: Average= Standard Score 90 to 109 (25^{th} to 74^{th} percentile); Low Average= Standard Score 80 to

89 (9th to 24th percentile); Below Average= (2nd to 8th percentile); Exceptionally low= (<2nd percentile). The data was then dichotomized to yes/no for (1) developmental delay, (2) global developmental delay, and (3) below average for each subject to facilitate harmonization between the two different test exams across both sites.

Mouse Screen Analysis

A retrospective analysis was carried out on the mouse lines described by Li et al.[72] In brief, a forward recessive mouse screen was carried out using N-ethyl-N-Nitrosourea in which 3700 mouse lines, defined by G1 sire, were screened for defects. Defect screening was completed through ultrasound scanning, micro-computed tomography (CT), micro-magnetic resonance imaging (MRI) and visual inspection of G3 offspring. Resulting mutant cardiac phenotypes were confirmed through necropsy, or histopathologic analysis. Further analysis was completed examining the craniofacial and gross brain abnormalities discovered within the screen. Lines in which a mutant was recovered in the original screen were analyzed for both craniofacial and gross brain abnormality. Consistent phenotype in at least three mice was required for a line to be considered abnormal with a craniofacial or brain abnormality. An additional mouse model which recapitulates the phenotype of Joubert syndrome was analyzed prior to any analysis on the main *Ohia* line to validate method and findings. The mouse model was previously validated by Damerla et al.[73] This Joubert syndrome mouse mode is colloquially called Heart Under Glass (*Hug*) and contains a S235P missense mutation in Jbts17. The *Hug* mice recapitulate the brain phenotype of Joubert syndrome presenting with decreased number of cerebellar fissures.

Episcopic Confocal Microscopy (ECM)

Head samples were removed following necropsy and fixed in 4% PFA solution for a minimum of 72 hours. After fixation, samples were prepared for ECM via three graded ethanol baths of 10%, 20%, and 40% overnight at room temperature. Samples were then transferred to a Sakura Tissue Tek VIP 5 Tissue Processor where they were dehydrated using increasing percentages of warmed ethanol baths and eventually perfused with paraffin wax. Samples were embedded in paraffin blocks to be sectioned coronally. 3D reconstructed images stacks were used for brain scoring and volumetric analysis. A diagram for the ECM workflow can be found in Supplemental Figure 4.

Mouse Brain Dysplasia Scoring

A group of three reviewers reviewed 84 cases consisting of 69 Ohia, five CRISPR/CAS9, and 10 wild type samples. Reviewers came to a consensus for each structure scored. In total seven structures were included the mouse brain scoring including hippocampus, cerebellum, cerebrum, left and right olfactory bulbs, brain stem, and midbrain. Hippocampus, cerebellum, and both olfactory bulbs were scored for aplasia, hypoplasia, and dysplasia. Cerebrum, brain stem and midbrain were scored for hypoplasia and dysplasia only. Each instance of abnormality received a binary score of zero or one. Brain Dysplasia Score (BDS) was a sum of each area of the brain. Two other BDS metrics were calculated, one being a binary scoring of any cerebellar or hippocampal abnormalities and the another being a binary score if any abnormality was present in the sample at all. Cerebellar folds were counted using a sagittal view in the middle slice of the brain.

Mouse Brain Segmentation

Tiff images were converted to NIFTI images using ITK-Snap and FSL. Images were down sampled 4x using FMIRB's Linear Registration Tool (FLIRT). Resulting images were manually segmented into 16 discreet structures using ITK-Snap. Structures segmented included right hippocampus, right olfactory bulb, right subcortical area, right cortex, intracranial space, midbrain, left hippocampus, left olfactory bulb, left subcortical area, left cortex, extra-axial space, cerebellum, pons, medulla, hypothalamus, and choroid plexus. Due to the required processing methods for ECM, CSF is removed from the brain and replaced with paraffin wax. The space voided of CSF has been labeled as intracranial space and extra-axial space. Structures above the tentorium were combined to form a supratentorial volume and an infratentorial volume was also calculated. Infratentorial volumes consisted of the pons, medulla, and cerebellum, while the supratentorial volumes were composed of the hippocampus, hypothalamus, olfactory bulbs, subcortical areas, cortex, and midbrain.

Genotype Analysis

We explored the relationship of Sap130/ Pcdha9 genotype and brain morphology in the mouse modeling. When comparing the risk stemming from the BDS for animals from the Ohia line, different genotypes were grouped into 6 distinct groups. Group A: *Sap130*(m/m) and *Pcdha9*(m/m), Group B: *Sap130*(m/m) and *Pcdha9*(m/+), Group C:

Sap130(m/m) and *Pcdha9*(+/+), Group D: *Sap130*(m/+) and *Pcdha9*(m/m), Group E: *Sap130*(+/+) and *Pcdha9*(m/m), and lastly, Group F: *Sap130*(m/+) or (+/+) and *Pcdha9*(m/+) or (+/+).

Mouse Genotype Groupings and Comparisons

For greater power in subsequent analysis, mice with similar genotypes were pooled into Groups. Group ABC consisted of mice which were homozygous mutant for *Sap130* (m/m), irrespective of their *Pcdha9* genotype. An additional Group, AB, contained mice which were homozygous mutant for *Sap130* (m/m), and either homozygous mutant or heterozygous for *Pcdha9* (m/*). To study the effect of homozygous mutations in the *Sap130* gene, Group ABC was compared against wildtype animals. Group ABC was then compared against Group F. Group F can only be heterozygous for *Sap130* and *Pcdha9*, so any effect of the homozygous mutant *Sap130* alleles would be removed in this group. This pairing should show effects of the homozygous *Sap130* mutation more concretely. To assess if any of the effect is coming from the *Pcdha9* genotype, Group AB was then compared to F. Group AB differs from Group ABC by removing samples that contained, wildtype *Pcdha9* genotyped animals. If *Pcdha9* is partially, or in large part, responsible for the observed phenotype, removing wildtype *Pcdha9* samples from the ABC Group should increase incidence and effects should become more significant. To further isolate the effect of *Sap130*, Group A was compared against Group C with the difference between groups being homozygous mutant *Pcdha9* (Group A) vs wildtype (Group C). Lastly, Group B was compared against Group D. Group B is homozygous *Sap130* and heterozygous *Pcdha9*, and Group D is the opposite, *Sap130* heterozygous, and *Pcdha9* homozygous mutant. If either homozygous gene is more significant than the other, the effect could be seen within this comparison.

RNAseq Analysis

RNA was isolated from brain tissue samples of 4 *Ohia* mutant animals and 5 littermate controls at embryonic day E13.5-E14.5, libraries were constructed and sequenced on the Illumina HiSeq 2000 platform (BGI Americas), and differential gene expression analysis was conducted as previously described (Gabriel et al. Biorxiv paper). The online Database for Annotation, Visualization, and Integrated Discovery (DAVID) was used to perform gene ontology (GO) functional enrichment analysis.

Statistical Analyses for Human Studies

Primary analysis: SAS statistical software was used to carry out human statistical analysis. Our primary analysis compared the derived BDS between neonates with CHD and controls**.** This analysis was performed using multivariate regression and three major co-variates were included in the model: gender, postconceptional age (PCA=gestational age plus postnatal age), time of MRI scan timing of scan relative to cardiac surgery (pre- vs post-operative). Multi-variate regression with false discovery rate (FDR) correction was used, to correct for multiple comparisons. The FDR is one way of conceptualizing the rate of type 1 errors in null hypothesis testing when conducting multiple comparisons. Whether BDS is association with sex difference, GA, or PCA was assessed in the entire study cohort.
Secondary analysis: Secondary analysis was repeated within the CHD only group, with birthweight and the presence of genetic abnormality included as additional comparisons with BDS. Furthermore, whether pre- or post-operative and pre-term or term status correlated with BDS was also analyzed within the CHD group. As an additional secondary analysis, within the CHD group, BDS was compared to the presence of various injuries and cortical maturation features. Additional secondary analyses including correlation of BDS with feeding data and neurodevelopmental outcome which consisted of linear and logistic regression with false discovery rate (FDR) correction for multiple comparisons; FDR-adjusted p-value <0.05 was considered significant.

Statistical Analyses for Mouse Studies

Volumetric analysis of mouse individual structures was carried out using SAS statistical software. Both raw and normalized by total brain volume values were compared in any models generated. We completed an ad hoc analysis to delineate the relationship between BDS and regional brain volumes, clinical risk factor and heart lesion subtypes on our primary outcome measures. Clinical variables were compared using a three-way ANCOVA (analysis of covariance) between wild-type, *Ohia*, and *Hug* animals. We then compared each of the groups mentioned above to each other using pairwise T-tests.

Role of Funders

Funding sources were not involved in patient recruitment, data collection, analysis, or formation of the manuscript. All work was original and completed by the authors without interaction by the funding sources.

Results

Comparison of Brain Injury/Cortical Maturation Score (TMS) between CHD and Control Cohorts:

The preterm CHD and term CHD cohort demonstrated increased incidence of brain injury compared to their gestational-aged, matched controls. Specifically, the CHD preterm cohort demonstrated increased incidence of focal infarcts ($p = 0.0295$) and punctate white matter lesions ($p = 0.0231$) compared to the preterm control cohort. The term CHD cohort demonstrated increased rates of hemorrhage ($p = 0.0284$), focal infarct ($p = 0.0035$), punctate white matter lesions ($p < 0.001$), dichotomized injury composite score ($p < 0.001$), and injury composite score ($p < 0.001$) compared to the term control cohort (Supplemental Table 1).

When comparing the categories of the cortical maturation score (TMS), the term CHD cohort had widespread reduced cortical maturation (in all cortical lobes except occipital) compared to term control cohort, while the preterm CHD only differed from preterm controls in the myelination category (Supplemental Table 2).

Derivation of Human BDS in Human Infant CHD:

There was a high incidence of olfactory, hippocampal, and cerebellar abnormalities in the preterm and term CHD cohorts compared to both preterm and term control cohorts respectively (Table 1). Within the univariate analyses, there was no significant correlation between BDS and sex, GA, or PCA within the entire study cohort (Table 2A). Within the CHD cohort, there was no correlation between BDS and pre/postoperative status, preterm/term status, or birth weight. Higher BDS in the CHD cohort was correlated with known genetic abnormalities (Table 2B), which remained a significant association in the multivariable analysis (Table 2C). BDS was highly correlated with cortical immaturity by cortical maturation scores including frontal cortex ($p < 0.0001$), insular cortex ($p < 0.0001$), and cortical folding ($p = 0.0016$), even after controlling for PCA at the scan (Table 3). There was no significant correlation between BDS and any categories of brain injury (Table 3). Within a subset of cases the inter-rater reliability was calculated and resulted in reviewers one and two receiving high scores for most metrics included in the BDS calculation. Notable exceptions were for cortical folding (kappa = 0.18, 0.00), myelination (kappa = 0.35, 0.02), supratentorial extra-axial fluid (kappa = 0.35, 0.05), and germinal matrix (kappa = 0.48, 0.00). Other values for Cohen's kappa measure for the BDS can be found in Supplemental Table 3.

Human Infant BDS and Regional Cerebral Volumes:

Higher BDS correlated with smaller left and total cerebellar volume, smaller deep grey matter and brain stem volumes, and increased infra-ventricular and supra-tentorial CSF volumes in the entire sample (term CHD and term control cohorts combined) (Table 4). Increased BDS was more strongly correlated with reduced cerebellar volume, reduced cortical volumes, and increased CSF volume in the term CHD cohort compared to the term control cohort (Table 4).

Human Infant BDS and Clinical Risk Factors:

When assessed against clinical risk factors in term CHD infants, the BDS did not correlate with birth factors, anthropomorphic data, cardiac lesion type, or intraoperative factors. (Supplemental Table 4A-D). The BDS did correlate with age of under 7 days at surgery ($p<0.048$, Supplemental Table 4B), increased length of hospitalization ($p<0.0447$, Supplemental Table 4D), and need for G-tube placement during the neonatal hospital stay ($p<0.01$, Supplemental Table 4D). Of note, we found no correlation between BDS and MRI field strength/scanner type (Supplemental Table 5).

Human Infant BDS and Feeding Outcomes:

Lack of oral feeding before neonatal hospital discharge was associated with multiple morphological abnormalities of the components of the BDS including cerebellar hemispheres and vermis, hippocampus, bilateral olfactory bulbs and olfactory sulci, corpus callosum, increased supratentorial extra-axial fluid, as well as total increased BDS. Hospital length of stay was associated with dysplasia of the cerebellar hemispheres and vermis, hippocampus, choroid plexus, brainstem, increased supratentorial axial fluid, and BDS. A diagnosis of dysphasia was associated with dysplasia of the brain stem ($p= 0.001$). Gastrointestinal dysmotility, aspiration, gastroesophageal reflux, malrotation, and vocal cord paralysis demonstrated no significant associations with brain dysplasia. Figure 2 panels A-D show some of the variations in hippocampal anatomy seen in the human population compared against that seen in the mouse in panels E and F. Figure 3 demonstrates olfactory bulb abnormalities in human infant CHD vs

control (A/C) and the mouse model (B/D) . Figure 4 demonstrates cerebellar abnormalities in the human infant CHD vs controls (A-top) and the mouse model (A-bottom).

Human Infant BDS and Neurodevelopmental Outcomes:

Increased BDS correlated with developmental delay in at least one domain including motor, cognitive, language/communication, or social/emotional ($p<0.02$), and specifically with poor expressive language development ($p < 0.016$) in a subset of the original sample tested at 15-18 months of age (n=90), given in Table 6.

Mouse CHD Screen Results

From the original mouse screen for CHD, 3208 mouse pedigrees were screened, and 390 (12.16%) mutant lines were discovered. Of the 390 mutant lines, 214/390 (54.87%) had some form of craniofacial anomaly and 69/390 (17.69%) lines had a severe brain anomaly. Within those categories, craniofacial and brain anomalies, 174/214 (81.31%) and 62/69 (89.86%) had co-occurrence of CHD, respectively. Supplemental Figure 5 demonstrates some of the craniofacial abnormalities seen during the screening. 68 lines contained features of both types of anomalies, and of those 68 lines, 61 also exhibited CHD. A summary of the results can be seen in Figure 5

Hug Model Mouse ECM Validation

To validate the ECM method, a mouse model, colloquially called Heart Under Glass or Hug, for Joubert syndrome with a S235P missense mutation in Jbts17 was analyzed prior to analysis of Ohia mice. Joubert syndrome is a ciliopathy associated with cerebellar abnormalities and other birth defects. In addition, Hug mice also had higher incidences of BDS ($p =0.0161$). and specifically, in the cerebellum-hippocampus dichotomized BDS ($p =0.0154$). Compared to wildtype mice, Hug mice showed an overall increase in cerebellar abnormalities ($p < 0.001$) and a decrease in the number of cerebellar fissures ($p= 0.0023$).

Ohia Mouse Model Brain Dysplasia Scoring

ECM analysis was completed on 69 Ohia mutant neonatal mice. There was an increase in the BDS in the Ohia group compared to the wildtype group ($p < 0.001$) (Table 7). With regards to individual subcortical abnormalities (which make up the composition of the BDS), the cerebellum showed the highest incidence of abnormality with dysplasia being present in 49/67 (73.13%) of animals scored and was highly significant compared to control animals ($p < 0.001$). Ohia mutants also showed a decrease in the number of cerebellar fissures ($p < 0.001$) compared to the wild type group. The Ohia mutants also showed an increase in incidence of hippocampal dysplasia ($p = 0.002$), cerebral dysplasia ($p = 0.003$), left olfactory bulb aplasia ($p = 0.024$), left olfactory bulb any abnormality ($p = 0.006$), right olfactory bulb aplasia ($p = 0.02$), and right olfactory bulb any abnormality ($p = 0.007$) (Table 7). Supplemental Figure 6 demonstrates some of the common phenotypes seen in Ohia mice. Findings of aplasia, hypoplasia or dysplasia were common in the olfactory bulb, cerebellum, and/or hippocampus. Additionally holoprosencephaly was a coincidental finding in Ohia mice with 42/69 (60.9%) showing some signs of holoprosencephaly. Supplemental Figure 7 shows Ohia animals and two examples of the holoprosencephaly observed in this population.

Ohia Brain Dysplasia Scoring within CHD Subgroupings

To examine the relationship between CHD lesions and brain dysmaturation, the co-occurrence of different brain anomalies and any form of CHD was compared. We compared within the Ohia cohort looking at BDS and cerebellar fissures and found that the presence of CHD increased the BDS and reduced cerebellar fissures ($p- < 0.001$) (Table 8). Looking at other forms of cardiac sub-lesions, there was no significant differences between BDS and cerebellar folds (Table 8).

In Ohia animals there were 10 brain structures which showed an increased incidence of abnormalities in animals with CHD. Those structures included hippocampal dysplasia ($p = 0.043$), cerebral hypoplasia ($p = 0.008$), cerebral dysplasia ($p < 0.001$), cerebellar dysplasia ($p < 0.001$), left olfactory bulb aplasia ($p < 0.001$), left olfactory bulb any abnormality ($p < 0.001$), right olfactory bulb aplasia ($p < 0.001$), right olfactory bulb any abnormality ($p < 0.001$), brainstem dysplasia ($p = 0.016$), and midbrain dysplasia ($p = 0.0062$) (Supplemental Table 6A). Comparing single versus biventricular morphology, defects were more common in the cerebellum in double ventricular mice ($p < 0.001$) (Supplemental Table 6A). When comparing conotruncal vs non-conotruncal defects, mice with conotruncal defects showed an increased in the occurrence of hypoplasia in the cerebrum ($p = 0.037$) (Supplemental Table 6B) Within cyanotic vs acyanotic cardiac defects, mice with acyanotic defects showed

increases in the incidence of left olfactory bulb hypoplasia (p = 0.018) and any defect in the cerebellum (p = 0.037). Lastly, looking at mice with and without arch obstructions, mice with arch obstruction showed an increase in the occurrence of any defect in the cerebellum (p = 0.048) (Supplemental Table 6B).

Ohia Mouse Model Regional Brain Volumes

Ohia mutants demonstrated a significant decrease in raw (non-normalized) volumes of the right subcortical (p = 0.044), left subcortical (p = 0.041), cerebellar (p = 0.005) and supratentorial volume (p = 0.037) volumes (non-normalized) compared to wild type control. Ohia mutants also demonstrated an increase in the intraventricular volume (p = 0.009) compared to wild type controls (Supplemental Table 7.

Normalizing volumes to total brain volume showed Ohia animals also exhibited a significant increase in medullary (p = 0.024) and intraventricular normalized volume (normalized to total brain volumes). (p = 0.015). Ohia animals also demonstrated a decrease in normalized supratentorial volumes (p = 0.01) compared to wild type controls (Supplemental Table 7).

Ohia Mouse Model Regional Brain Volumes within CHD Subgroupings

There were no differences in raw (non-normalized) volumes between Ohia mice with and without CHD. Looking at single versus biventricular morphology, mice with biventricular heart defects showed increases in the volumes of the right subcortical areas (p = 0.006), left subcortical area (p = 0.036), and the pons (p = 0.024) (Supplemental Table 8a). Comparing conotruncal against non-conotruncal heart defects, mice with conotruncal defects showed an increased in the right subcortical area (p = 0.043) (Supplemental Table 8b). Mice with acyanotic defects demonstrated an increase in the volume of the left hippocampus (p = 0.044) (Supplemental Table 8b). There were no differences in volume noticed between mice with and without arch obstructions.

After normalizing raw volumes to total brain volume different regions showed significance between groups. Between CHD and non-CHD Ohia mice, Ohia mice with CHD showed increased volumes in the right cortex (p = 0.026), midbrain (p = 0.044) and cerebellum (p = 0.044). Comparing normalized volumes within single and biventricular groupings found that single ventricular morphology heart defect mice had increased choroid plexus volumes (p < 0.001). (Supplemental Table 9a). There were no significant findings looking between groups of conotruncal vs non-conotruncal, cyanotic vs acyanotic, or arch obstruction vs no arch obstruction (Supplemental Table 9b).

Ohia Mouse Model Brain Dysplasia Scoring within Genotype Subgroupings

Comparing genotypes within the Ohia cohort, samples were first grouped based on genotypes. The two groups with the most samples were group A which consisted of Sap130 and Pcdha9 double mutants and group F consisted of animals which did not have a Sap130 or Pcdha9 homozygous mutant genotype (Table 9). Both groups showed high incidence rates of olfactory bulb, cerebellar, hippocampal, and brainstem abnormalities (Table 9). Using Group ABC mentioned in the Mouse Genotype Groupings section in the methods, values of hippocampus and cerebellar BDS (p < 0.001) and BDS total (all structures) were greater (p < 0.001) in Group ABC compared to wildtype (Table 10).

Within the different genotype groups there were various findings. Groups A and B had 19/24 (79.17%) and 6/8 (75%) of mice exhibiting some form of holoprosencephaly. Additionally, those groups had the high rates of CHD and the various subtypes of CHD (i.e., conotruncal, single ventricular morphology, cyanotic defects, and arch obstructions) (Supplemental Table 10.

When comparing ABC vs WT, to determine homozygous Sap130 mutation difference compared to controls, 10 structures studied showed greater incidence values in ABC compared to wildtype. Those structures included dysplastic hippocampus (p < 0.001), hypoplastic cerebrum (p = 0.40), dysplastic cerebrum (p < 0.001), dysplastic cerebellum (p < 0.001), aplastic left olfactory bulb (p = 0.001), combination of left olfactory bulb (p < 0.001), aplastic right olfactory bulb (p = 0.001), combination of right olfactory bulb (p = <0.001), dysplastic brainstem (p = 0.037), and the dichotomized BDS (p = <0.001) (Supplemental Table 7a).

Comparing groups ABC vs. F to determine homozygous Sap130 mutation difference compared to no homozygous mutation in either gene (at most hetero or WT for either mutation), hippocampal and cerebellar BDS was different between groups with ABC, a higher incidence (p = 0.008) (Table 10). Eight structures had significantly increased incidence in group ABC compared to F. Structures included hypoplastic cerebrum (p = 0.021), dysplastic cerebrum

(p = 0.016), dysplastic cerebellum (p < 0.001), aplastic left olfactory bulb (p = 0.035), combination of left olfactory bulb (p = 0.010), aplastic right olfactory bulb (p = 0.022), combination of right olfactory bulb (p = 0.018), and dichotomized BDS (p = 0.021). Additionally, the ABC group had an increased value for the hippocampus and cerebellum BDS (p = 0.008) (Supplemental Table 7a).

In comparing groups AB vs. F, (homozygous Sap 130 mutation and homo/heteroPCDHA9 vs no hippocampal and cerebellar BDS was significantly different between groups (p 0.021) (Table 10). Seven structures showed significant differences in the rate of abnormalities; structures included hypoplastic cerebrum (p = 0.035), dysplastic cerebrum (p = 0.019), dysplastic cerebellum (p = 0.001), aplastic left olfactory bulb (p-value = 0.039), combination of left olfactory bulb (p = 0.023), aplastic right olfactory bulb (p = 0.023), and combination of right olfactory bulb (p = 0.023) (Supplemental Table 7b). Comparing groups A vs C, only 2 structures were found significant. Those structures were dysplastic brainstem (p = 0.028) and dysplastic midbrain. (p = 0.042) (Supplemental Table 7b). Comparing groups B vs D, only aplastic hippocampus (p 0.029) and any defect in hippocampus (p = 0.014) were found to be significant (Supplemental Table 7c).

Ohia Mouse Model Regional Brain Volumes within Genotype Subgroupings

Looking at volumes for brain regions between genotype groups, in group ABC vs wild type, six areas were found to be significantly different with mice in group ABC having reduced volumes including the right subcortical area (p = 0.006), right cortex (p = 0.047), left subcortical area (p = 0.007), cerebellum (p-value = 0.003), supratentorial volume (p =0.013), and total brain volume (p = 0.028) (Supplemental Table 11a).

In group ABC vs F, mice in group ABC showed significant volume reductions in eight structures. Structures included right hippocampus (p-value = 0.041), right subcortical areas (p = 0.050), right cortex (p = 0.016), left hippocampus (p-value = 0.031), left olfactory bulb (p = 0.048), left cortex (p = 0.022), supratentorial volume (p-value = 0.018), and total brain volume (p = 0.022) (Supplemental Table 11a). Similarly comparing groups AB vs. F, mice in group AB showed significant reductions in volumes in eight structures. Differences occurred between right hippocampus (= 0.021), right subcortical areas (p-value = 0.023), right cortex (p = 0.029), left hippocampus (p-value = 0.024), left subcortical areas (p =0.038), left cortex (p =0.029), supratentorial volume (p =0.014) and total brain volume (p = 0.014) (Supplemental Table 11b). Lastly, comparing group A vs C, animals in group A showed significant reductions in four areas including the right subcortical area (p =0.022), left subcortical area (p =0.034), infratentorial volume (p =0.047), total brain volume (p =0.049) (Supplemental Table 11b).

After normalizing raw volumes to total brain volume, multiple brain regions showed significant differences between groupings. The ABC group demonstrated increased volume of the midbrain (p = 0.027) and medulla (p = 0.005) and decreased volume of the right olfactory bulb (p = 0.037) and supratentorial region (p = 0.009) compared to the wild type groups (Supplemental Table 12a). The ABC group demonstrated significant increases in volume in three areas including the cerebellum (p = 0.010), medulla (p = 0.043), and choroid plexus (p = 0.012) compared to the F group. Additionally, the right cortex volume was reduced in animals in group ABC compared to F (p = 0.028) (Supplemental Table 12a).

Comparing groups AB vs F, mice in group AB demonstrated three structures with significant increases in volume including the cerebellum (p = 0.012), pons (p = 0.049), and choroid plexus (p = 0.029). There were no significant differences between groups A vs C and B vs D (Supplemental Table 12b).

Mouse CHD/Ohia RNA-seq

RNA-seq transcriptome profiling in term Ohia brains showed changes in genes involved in learning and memory, feeding behaviors, neuronal differentiation, and synaptic transport (Figure 6) Sap130 chromatin immunoprecipitation sequencing (CHIP-seq) looking at targets associated with Sap130 in brain tissue revealed a total of 644 genes being associated with cardiac and brain associated genes. Of those 644 genes, 106 and 324 were cardiac and brain genes, respectively, with the remaining 214 genes being associated with both brain and cardiac. The top three phenotypes associated with the Sap130 CHIP-seq analysis were global brain delay, abnormal brain development, and abnormal nervous system development.

Crisper/CAS Phenotype Validation

Crisper/CAS9 mice were also processed via ECM for validation of phenotype associated with Ohia mice. Three different crisper/CAS mice were developed to validate, a Sap130/Pcdha9 double mutant, Sap130 only and Pchda9 only. Brain scoring was performed like Ohia mice and findings support a similar phenotype. In the Sap130/Pcdha9

608 double mutant mice analyzed, they were found to exhibit a severe phenotype characterized by smoothed
609 cerebellum, aplastic or highly dysplastic olfactory bulbs, and aplastic hippocampus. Other animals showed a
610 pattern of holoprosencephaly. The Sap130 crisper animal showed a severe phenotype as well with smooth
611 cerebellum, absent or extremely abnormal olfactory bulbs, and either holoprosencephaly or an abnormal
612 hippocampus. In the Pcdha9 crisper animal, the phenotype was milder and presented with a cerebellum that while
613 dysplastic did present with fissures unlike the double mutant or Sap130 crisper animal, a semi-normal appearing
614 olfactory bulb and hippocampus. The phenotype was more severe in animals having mutations in the Sap130 gene.
615 A visual representation of the defects found in Crisper/CAS9 mice can be found in Supplemental Figure 8. A
616 similar pattern of severe olfactory bulb and hippocampal structural abnormalities was seen in our human
617 population. Supplemental Figure 9 shows the Crisper/CAS animals compared to a human subject with severe brain
618 dysmaturation.

619

Discussion

Our study validates a paralimbic related subcortical based semi-quantitative BDS, which has proven to be sensitive to dysmaturational differences between CHD and control infants as well as sensitive to neurodevelopmental outcomes within CHD infants, including associations with early language, clinical and feeding outcomes. Most conventional semi-quantitative MRI scoring systems in CHD patients have exclusively focused on either acquired brain injury or cortical maturation assessment, particularly in the neonatal period.[26-33] In this study, we demonstrated that not only is it possible to generate a paralimbic-related subcortically informed scoring system, but that such a scoring system holds important information regarding outcomes for CHD infants at risk for atypical neurodevelopment. The key subcortical components of our scoring system included subcortical structures that are known to be part of para-limbic neural networks including the olfactory bulb, the hippocampus, the cerebellum and the deep grey structures like the striatum. Furthermore, we showed that there is a distinct similarity between findings seen in CHD infants when compared to a preclinical mouse model of CHD suggesting similar mechanisms of brain dysmaturation.

In our study, we found a high incidence of paralimbic related subcortical abnormalities including olfactory, cerebellar, hippocampal, and brainstem abnormalities in infants with CHD compared to controls. We found similar olfactory bulb defects in the preclinical mouse model that we also see in our human CHD population. These abnormalities were used to derive a semi-quantitative subcortical abnormality or brain dysplasia score (BDS). We found that this BDS correlated with reduced cortical maturation (measured with the classic TMS), increased CSF volume and increased deep grey volume (striatum/thalamus). In contrast, the BDS did not correlate with GA, preterm status, cardiac lesion subtype, birth factors, intraoperative factors, or different vendor MRI/field strength. BDS did correlate with developmental delay and poor expressive language development. The BDS also correlates with age at surgery, increased length of hospitalization and need for G-tube placement. A more detailed evaluation of factors surrounding feeding and individual brain dysplasia parameters found correlations between lack oral feeding prior to neonatal hospital discharge and dysplasia of multiple brain areas as well as the BDS, and additionally with hospital length of stay which is likely the sequala of feeding dysfunction. Interestingly, swallowing dysfunction was associated with dysplasia of the brain stem.

An important component of our paralimbic-related subcortical BDS scoring system is the hippocampus. We found a consistent pattern of dysmaturation in the hippocampus, including severe forms of hippocampal aplasia or dysplasia in both mice and human subjects. Research has indicated that reductions in hippocampal volume and functional correlates in adolescents and adults resulted in an increased rate of neurodevelopmental impairment [74,75]. Fontes et. al found that hippocampal shape and volumetric abnormalities found within CHD subjects can be predictive of impaired executive function. It is possible that the hippocampus is particularly vulnerable to early injury in CHD individuals as it is a brain region particularly susceptible to injury related to hypoxemia or hemodynamic instability. Latal et al found that reductions in hippocampal volume correlated with reductions in total IQ, working memory, and verbal comprehension. Lastly, one study looking at maternal stress found that reductions in hippocampal volumes are present in utero, consistent with previous volumetric findings of CHD[76]. Wu et. al concluded that universal screening looking at maternal stress is important, as early identification of hippocampal abnormalities is imperative.

Another important component of our paralimbic-related subcortical scoring system was the cerebellum. Cerebellar dysfunction has been linked with adverse neurodevelopmental outcomes[77-79]. Stoodley found that cerebellar damage or malformation present in early stages of development to be more detrimental than when obtained in adulthood, and theorized that injuries could affect cerebral-cerebellar circuits that are crucial to development and learning.[78] Zwicker et. al found that preterm infants with exposure to morphine in the neonatal period had decreased cerebellar volumes and worse neurodevelopmental outcomes.[79] Additionally, our group has previously shown that CHD children with reduced cerebellar volumes scored worse in tests for working memory, inhibitory control, and mental flexibility[80]. We also demonstrated that the superior surface of the cerebellum, primarily composed of the posterior lobe and the midline vermis, is an area particularly susceptible to alterations in morphology, indicating possible regions specifically affected by dysmaturation in CHD.[35] Previous literature in combination with our BDS findings show the importance of the cerebellum toward neurodevelopment and suggest that insults or injury affecting proper cerebellar development may impact neurodevelopmental outcomes. Figure 4 demonstrates some of the commonalities seen between the mouse and human cerebellum; of note are the abnormal number cerebellar fissure and small size.

An important subcortical structure that was noted to be abnormal in the human BDS score volumetric correlation analysis and in the preclinical modeling was the striatum. In infancy, striatal connectivity is related to later motor and affective outcomes[81-83], with previous research suggesting there are abnormalities in CHD[84], potentially linking disrupted development with future behavior. The striatum forms a neural network with indirect and direct connectivity with other subcortical paralimbic components of the BDS score including the cerebellum, hippocampus and olfactory bulb. As such the developing striatum is part of a dense, interconnected network that supports motor function, reward processing, and cognition[85,86], with circuitry specialized for affective based learning and olfactory reward. Supported by work in animal models and adults, the olfactory bulb directly projects to the olfactory tubercle[87], a part of the ventral striatum, specialized for olfaction and containing significant dopamine neurons[88,89]. Together with innervations to the striatum from the hippocampus and amygdala[90-93], the ventral striatum has been suggested to represent odor valence cues and instigate goal-directed behavior[87], facilitated by additional input from piriform cortex and prefrontal cortex[94-96]. Output from the ventral striatum proceeds to the pallidum and then the thalamus, which then closes the feedback loop with prefrontal cortex[97,98]. An important structure in this loop is the orbitofrontal cortex, which plays an important role in maintaining changing odor representations but also more broadly in decision making and stimulus evaluation[99]. Integrated into these loops are other subcortical structures, including the cerebellum, which also has a significant role in movement and more recently emphasized role in cognition and language[100]. Through the thalamus and pons, the cerebellum indirectly projects to putamen, pallidum and the subthalamic nucleus[101,102]. These outputs may be topographically organized, converging on both the ventral striatum and frontal areas, with suggested involvement in appetitive reward[103] and strategic motor learning[104]. Disruption of this interconnected network is likely captured by BDS scores, which are then sensitive to striatally relevant neurodevelopmental outcomes.

Within the *Ohia* mouse model the two main driver genes were *Sap130* and *Pcdha9*, and while both genes were necessarily to have cardiac phenotype, both genes were not required to have neuroanatomic abnormalities. Additionally, *Sap130* mutations presented with a more severe brain phenotype compared to *Pcdha9* mutations. This is interesting as knock-out mice for *Sap130* are embryonically lethal whereas *Pcdha9* knock-out mice are viable suggesting that *Sap130* may have a more upstream effect whereas *Pcdha9* is more downstream.[105] *Sap130* functions as a subunit of the histone deacetylase dependent co-repressor complex which has roles transcriptional regulation and has been specifically mentioned to be required for recovery from hypoxia.[106] *Pcdha9* is a member of the protocadherin alpha gene cluster which are important plasma membrane proteins for cell-cell connections, neural projects, and synapse formation.[107] Interestingly both genes show overlap in connectomes with chromatin and histone modification pathways.[44] Alterations in histone modifying pathways have been linked to various forms of CHD. [108-110] It's likely that there are many other genes and gene pairings that could cause a similar neurodevelopmental phenotype as it's possible the main driver could be epigenetic dysregulation resulting in altered differential expression of genes required for signaling and migration. Incorrect timing for migrating neural cells might explain why preterm babies and CHD babies look phenotypically similar in regard to neurodevelopment. Looking at the genetics of the preclinical mouse model could not be conclusive as to the etiology of the human CHD neurodevelopmental issues; however, we demonstrate spectra of cardiac and brain anatomical abnormalities associated with the different genetic combinations of the *Ohia* mouse, parallel to those seen in human subjects.

CHD subjects have a documented risk of poor neurodevelopmental outcomes although the specific mechanism is unknown.[111-115] Additionally, neurodevelopmental impairments can continue to affect individuals well past infancy and into adolescence and early adulthood.[116-121] There are two main hypotheses with regard to the origin of injury to the brain and subsequent neurodevelopmental deficits that arise from the injury; intrinsic patient factors including genetics or altered substrate delivery due to the cardiac malformation. There have been studies looking at the heritability of CHD to determine the genetic causes which resulted in the finding that CHD most likely has a genetic component. CHD is particularly common in genetic syndromes caused by aneuploidy defects; ranging anywhere from 20% - 100% of individuals with trisomies 13, 18, and 21 as well as and monosomy X[122], though these syndromic cases account for a relatively low amount of the total CHD population. Additionally, rates of CHD are increased when there are abnormal chromosomal structural syndromes such as deletions, insertions, and copy number variants.[123] Known de novo single nucleotide polymorphisms account for approximately 10% of CHD cases, roughly the same amount that can be attributed to environmental factors.[123,124] However, the vast majority of CHD individuals have an unknown origin of the cardiac defect as well as subsequent neurodevelopmental abnormalities. To overcome this missing data, work has begun looking at previously uncharacterized de novo mutations in mice, singling out genes with human homologs and which have high

expression in the heart. When looking at only the homologous genes, researchers found that between CHD and control individuals, there was no significant difference between rates of generic de novo mutations; however, when comparing genes with high cardiac expression, CHD subjects had much higher rates of mutations in protein-altering mutations.[125] This recent work into the genetic origins of CHD has shown that even when the cause of the insult is unknown, the cause of CHD is likely genetic possibly through the alteration of genes which affect similar downstream pathways.

Whether the genetic insult is the main driver or whether the mutations leave the individual susceptible to other forms of injury is unknown. Our group has previously looked at how the developing subcortical paralimbic-related structures of the brain can be linked to energy metabolism and found that subcortical morphological differences were not likely linked to prematurity or white matter injury alone, but that there was a linkage between brain metabolism and subcortical structural morphometry.[58] Stemming from these findings, we believe that subplate vulnerability in the prenatal and immediate post-natal period can be informative to understanding the subcortical dysmaturation seen in CHD infants. Within CHD individuals, it's been shown that preoperatively they have volumetric abnormalities present in the cerebellum and brainstem[16] and additionally that abnormal cerebellar growth has been linked with worse outcomes in expressive communication and the adaptive development quotient in CHD individuals.[12] Furthermore, there is an established link between subcortical morphological abnormalities and white matter vulnerability which can lead to injury and eventual worse neurodevelopmental outcomes.[17,20] With the mounting evidence of the importance of subcortical structures for proper brain development, and the subcortical structures' relationship to proper cortical development, inclusion of subcortical structures into our scoring system is necessary to characterize the entire picture of brain dysplasia. With nearly half of CHD cases still without a known genetic origin, identifying subtle cases of neurodevelopmental abnormalities in CHD individuals can better help us understand the downstream effects of CHD on brain development, ultimately furthering knowledge of the interplay between CHD and neurodevelopmental outcomes. Importantly, early interventional strategies have shown promise in helping CHD individuals with potential neurocognitive difficulties[126] and early identification of the most vulnerable through proper screening is necessary to identify and target therapies toward highest risk individuals.

Limitations

Our study does have some important limitations. The preterm and term CHD cohorts that we studied were heterogenous related to heart lesion subtypes. During this study, only a limited number of socio-demographic factors were prospectively collected and therefore analysis using these factors was unable to be carried out and future work correlating BDS score with pediatric/adolescent neurocognitive outcomes in relation to socio-demographic factors is needed. Our multi-site approach with different scanner platforms and vendors can lead to interscanner variance, but our secondary analyses did not find a correlation between scanner vendor or field strength and brain dysplasia score. Future work employing retrospective machine learning techniques like the empirical Bayes technique (Combat) can be used to reduce interscanner variance. Importantly, we were not able to measure extra-axial CSF fluid in the ECM imaging of the mouse mutants, which is an important component of the BDS score. Complete removal of CSF and infiltration of paraffin could have altered CSF volumes or the ventricle shape. With this in mind, we did not feel comfortable labeling these brain regions as containing CSF and instead labeled them as extra-axial space.

Contributors

Conceptualization: WTR, JVS, GG, VL,

Data Curation: WTR, JVS, GG, VL,

Manuscript Draft Preparation: WTR, JVS, GG, VL,

Manuscript Editing: WTR, JVS, GG, VL,

Statistical Analysis: VL, VS

Human Quantitative Scoring and Reads: SS, AP

Human Volumetric Segmentation: WTR,

Human Cardiac Lesion Characterization: JVS,

Mouse Quantitative Scoring: WTR, YW, AP

Mouse Volumetric Segmentation: RS,AP

Supervision: CL, AP

Verification of Underlying Data: WTR

Declaration of Interests

The authors declare that there are no conflicts of interest.

Acknowledgments

This work was supported by the Department of Defense (W81XWH-16-1-0613), the National Heart, Lung, and Blood Institute (R01 HL152740-1, R01 HL128818-05), and the National Heart, Lung and Blood Institute with National Institute on Aging (R01HL128818-05 S1). Southern California Clinical and Translational Sciences Institute (NCATS) through Grant UL1TR0001855. Its contents are solely the responsibility of the authors and do not necessarily represent the official views of the NIH. We also acknowledge Additional Ventures for support (AP, VR, RC). VR is supported by the Saban Research Institute, Additional Ventures Foundation and NIH-NHLBI K01HL153942. NT is supported by Children's Hospital Los Angeles Clinical Services Research Grant and the NINR K23 Grant 1K23NR019121-01A1.

Data Sharing Statement

Preclinical mouse data can be made available upon request to corresponding author. Clinical data cannot be made public due to privacy issues, but limited data can be made available upon special request to the corresponding author with justification for the data request.

References

1. Hoffman JI, Kaplan S. The incidence of congenital heart disease. *J Am Coll Cardiol* 2002; **39**(12): 1890-900.

2. Sun R, Liu M, Lu L, Zheng Y, Zhang P. Congenital Heart Disease: Causes, Diagnosis, Symptoms, and Treatments. *Cell Biochemistry and Biophysics* 2015; **72**(3): 857-60.

3. Rollins CK, Newburger JW, Roberts AE. Genetic contribution to neurodevelopmental outcomes in congenital heart disease: are some patients predetermined to have developmental delay? *Current Opinion in Pediatrics* 2017; **29**(5): 529-33.

4. Jin SC, Homsy J, Zaidi S, et al. Contribution of rare inherited and de novo variants in 2,871 congenital heart disease probands. *Nature Genetics* 2017; **49**(11): 1593-601.

5. Homsy J, Zaidi S, Shen Y, et al. De novo mutations in congenital heart disease with neurodevelopmental and other congenital anomalies. *Science* 2015; **350**(6265): 1262-6.

6. Ji W, Ferdman D, Copel J, et al. De novo damaging variants associated with congenital heart diseases contribute to the connectome. *Scientific Reports* 2020; **10**(1).

7. Hayek C, Rajagopalan V, Meouchy J, et al. Ventricular and total brain volumes in infants with congenital heart disease: a longitudinal study. *Journal of Perinatology* 2020; **40**(9): 1383-8.

8. Bonthrone AF, Dimitrova R, Chew A, et al. Individualized brain development and cognitive outcome in infants with congenital heart disease. *Brain Commun* 2021; **3**(2): fcab046.

9. Bonthrone AF, Kelly CJ, Ng IHX, Counsell SJ. MRI studies of brain size and growth in individuals with congenital heart disease. *Translational Pediatrics* 2021; **10**(8): 2171-81.

10. Stinnett GR, Lin S, Korotcov AV, et al. Microstructural Alterations and Oligodendrocyte Dysmaturation in White Matter After Cardiopulmonary Bypass in a Juvenile Porcine Model. *Journal of the American Heart Association* 2017; **6**(8): e005997.

11. Morton PD, Korotcova L, Lewis BK, et al. Abnormal neurogenesis and cortical growth in congenital heart disease. *Science translational medicine* 2017; **9**(374): eaah7029.

12. Wong A, Chavez T, O'Neil S, et al. Synchronous Aberrant Cerebellar and Opercular Development in Fetuses and Neonates with Congenital Heart Disease: Correlation with Early Communicative Neurodevelopmental Outcomes, Initial Experience. *American Journal of Perinatology Reports* 2017; **7**(01): e17-e27.

13. von Rhein M, Buchmann A, Hagmann C, et al. Brain volumes predict neurodevelopment in adolescents after surgery for congenital heart disease. *Brain : a journal of neurology* 2014; **137**(Pt 1): 268-76.

14. von Rhein M, Buchmann A, Hagmann C, et al. Severe congenital heart defects are associated with global reduction of neonatal brain volumes. *The Journal of pediatrics* 2015; **167**(6): 1259-63. e1.

15. Owen M, Shevell M, Donofrio M, et al. Brain volume and neurobehavior in newborns with complex congenital heart defects. *J Pediatr* 2014; **164**(5): 1121-7 e1.

16. Ortinau C, Beca J, Lambeth J, et al. Regional alterations in cerebral growth exist preoperatively in infants with congenital heart disease. *The Journal of Thoracic and Cardiovascular Surgery* 2012; **143**: 1264-70.

17. Volpe JJ. Brain injury in premature infants: a complex amalgam of destructive and developmental disturbances. *Lancet neurology* 2009; **8**(1): 110-24.

18. Volpe JJ. Brain injury in the premature infant: overview of clinical aspects, neuropathology, and pathogenesis. *Seminars in Pediatric Neurology* 1998; **5**: 135-51.

19. Ligam P, Haynes RL, Folkerth RD, et al. Thalamic damage in periventricular leukomalacia: novel pathologic observations relevant to cognitive deficits in survivors of prematurity. *Pediatr Res* 2009; **65**(5): 524-9.

20. Wisnowski JL, Ceschin RC, Choi SY, et al. Reduced thalamic volume in preterm infants is associated with abnormal white matter metabolism independent of injury. *Neuroradiology* 2015; **57**(5): 515-25.

21. Panigrahy A, Lee V, Ceschin R, et al. Brain Dysplasia Associated with Ciliary Dysfunction in Infants with Congenital Heart Disease. *The Journal of Pediatrics* 2016; **178**: 141-8. e1.

22. Ceschin R, Zahner A, Reynolds W, et al. A computational framework for the detection of subcortical brain dysmaturation in neonatal MRI using 3D Convolutional Neural Networks. *NeuroImage* 2018; **178**: 183-97.

23. Heye KN, Knirsch W, Latal B, et al. Reduction of brain volumes after neonatal cardiopulmonary bypass surgery in single-ventricle congenital heart disease before Fontan completion. *Pediatric research* 2018; **83**(1): 63-70.

24. von Rhein M, Buchmann A, Hagmann C, et al. Severe congenital heart defects are associated with global reduction of neonatal brain volumes. *The Journal of pediatrics* 2015; **167**(6): 1259-63. e1.

25. Watson CG, Stopp C, Wypij D, Newburger JW, Rivkin MJ. Reduced cortical volume and thickness and their relationship to medical and operative features in post-Fontan children and adolescents. *Pediatric research* 2017; **81**(6): 881-90.

26. Alablani FJ, Chan HSA, Beishon L, et al. Paediatric brain MRI findings following congenital heart surgery: a systematic review. *Archives of disease in childhood* 2022; **107**(9): 818-25.

27. Bhattacharjee I, Mohamed MA, Nandakumar V, Friedman NR, Ruggieri P, Aly H. Scoring of brain magnetic resonance imaging and neurodevelopmental outcomes in infants with congenital heart disease. *Early human development* 2022; **169**: 105574.

28. Brossard-Racine M, du Plessis A, Vezina G, et al. Brain injury in neonates with complex congenital heart disease: what is the predictive value of MRI in the fetal period? *Am J Neuroradiol* 2016; **37**(7): 1338-46.

29. Dijkhuizen EI, de Munck S, de Jonge RCJ, et al. Early brain magnetic resonance imaging findings and neurodevelopmental outcome in children with congenital heart disease: A systematic review. *Developmental Medicine & Child Neurology* 2023.

30. Li Y, Yin S, Fang J, et al. Neurodevelopmental delay with critical congenital heart disease is mainly from prenatal injury not infant cardiac surgery: current evidence based on a meta‐analysis of functional magnetic resonance imaging. *Ultrasound in Obstetrics & Gynecology* 2015; **45**(6): 639-48.

31. McCarthy AL, Winters ME, Busch DR, et al. Scoring system for periventricular leukomalacia in infants with congenital heart disease. *Pediatric research* 2015; **78**(3): 304-9.

32. Mulkey SB, Swearingen CJ, Melguizo MS, et al. Multi-tiered analysis of brain injury in neonates with congenital heart disease. *Pediatric cardiology* 2013; **34**: 1772-84.

33. Stegeman R, Feldmann M, Claessens NHP, et al. A uniform description of perioperative brain MRI findings in infants with severe congenital heart disease: results of a European collaboration. *Am J Neuroradiol* 2021; **42**(11): 2034-9.

34. Panigrahy A, Lee V, Ceschin R, et al. Brain Dysplasia Associated with Ciliary Dysfunction in Infants with Congenital Heart Disease. *The Journal of pediatrics* 2016.

35. Ceschin R, Zahner A, Reynolds W, et al. A computational framework for the detection of subcortical brain dysmaturation in neonatal MRI using 3D Convolutional Neural Networks. *NeuroImage* 2018.

36. Gabriel GC, Salamacha N, Reynolds WT, et al. Characterization of Neurodevelopmental Defects Associated With a Mouse Model of Hypoplastic Left Heart Syndrome. *Circulation* 2018; **138**(Suppl_1): A16609-A.

37. Panigrahy A, Ceschin R, Lee V, et al. Respiratory Ciliary Motion Defect Predict Regional Brain Abnormalities and Increased Extra Axial CSF Fluid in Neonates With Complex Congenital Heart Disease. *Circulation* 2014; **130**(Suppl 2): A16570-A.

38. Panigrahy A, Votava-Smith J, Lee V, et al. Abnormal Brain Connectivity and Poor Neurodevelopmental Outcome in Congenital Heart Disease Patients With Subtle Brain Dysplasia. *Circulation* 2015; **132**(Suppl 3): A16541-A.

39. Subramanian S, Soundara Rajan D, Gaesser J, Wen-Ya Lo C, Panigrahy A. Olfactory bulb and olfactory tract abnormalities in acrocallosal syndrome and Greig cephalopolysyndactyly syndrome. *Pediatric Radiology* 2019; **49**(10): 1368-73.

40. Votava-Smith JK, Schmithorst VJ, Tran N, et al. Impaired Pre-Operative Cerebral Autoregulation is Associated With Functional Brain Dysmaturation in Neonatal Congenital Heart Disease. *Circulation* 2017; **136**(suppl_1): A15580-A.

41. Votava-Smith JK, Gaesser J, Harbison AL, et al. Clinical factors associated with microstructural connectome related brain dysmaturation in term neonates with congenital heart disease. *Frontiers in neuroscience* 2022; **16**: 952355.

42. Limperopoulos C, Tworetzky W, McElhinney DB, et al. Brain volume and metabolism in fetuses with congenital heart disease: evaluation with quantitative magnetic resonance imaging and spectroscopy. *Circulation* 2010; **121**: 26-33.

43. Sun L, Macgowan CK, Sled JG, et al. Reduced fetal cerebral oxygen consumption is associated with smaller brain size in fetuses with congenital heart disease. *Circulation* 2015; **131**: 1313-23.

44. Liu X, Yagi H, Saeed S, et al. The complex genetics of hypoplastic left heart syndrome. *Nature genetics* 2017; **49**(7): 1152-9.

45. Thu CA, Chen WV, Rubinstein R, et al. Single-cell identity generated by combinatorial homophilic interactions between α, β, and γ protocadherins. *Cell* 2014; **158**(5): 1045-59.

46. Mountoufaris G, Chen WV, Hirabayashi Y, et al. Multicluster Pcdh diversity is required for mouse olfactory neural circuit assembly. *Science* 2017; **356**(6336): 411-4.

47. Anitha A, Thanseem I, Nakamura K, et al. Protocadherin α (PCDHA) as a novel susceptibility gene for autism. *Journal of Psychiatry and Neuroscience* 2013; **38**(3): 192-8.

48. Witteveen JS, Willemsen MH, Dombroski TC, et al. Haploinsufficiency of MeCP2-interacting transcriptional co-repressor SIN3A causes mild intellectual disability by affecting the development of cortical integrity. *Nature Genetics* 2016; **48**(8): 877-87.

49. Amir RE, Van den Veyver IB, Wan M, Tran CQ, Francke U, Zoghbi HY. Rett syndrome is caused by mutations in X-linked MECP2, encoding methyl-CpG-binding protein 2. *Nature genetics* 1999; **23**(2): 185-8.

50. Ballas N, Grunseich C, Lu DD, Speh JC, Mandel G. REST and its corepressors mediate plasticity of neuronal gene chromatin throughout neurogenesis. *Cell* 2005; **121**(4): 645-57.

51. Gao Z, Ure K, Ding P, et al. The master negative regulator REST/NRSF controls adult neurogenesis by restraining the neurogenic program in quiescent stem cells. *Journal of Neuroscience* 2011; **31**(26): 9772-86.

52. Wisnowski JL, Schmithorst VJ, Rosser T, et al. Magnetic resonance spectroscopy markers of axons and astrogliosis in relation to specific features of white matter injury in preterm infants. *Neuroradiology* 2014; **56**: 771-9.

53. Wisnowski JL, Bluml S, Paquette L, et al. Altered Glutamatergic Metabolism Associated with Punctate White Matter Lesions in Preterm Infants. *Plos One* 2013; **8**(2).

54. Blüml S, Wisnowski JL, Nelson MD, Paquette L, Panigrahy A. Metabolic maturation of white matter is altered in preterm infants. *Plos One* 2014; **9**: e85829.

55. Blüml S, Wisnowski JL, Nelson Jr MD, Paquette L, Panigrahy A. Metabolic maturation of white matter is altered in preterm infants. *Plos One* 2014; **9**(1): e85829.

56. Blüml S, Wisnowski JL, Nelson MD, et al. Metabolic maturation of the human brain from birth through adolescence: insights from in vivo magnetic resonance spectroscopy. *Cerebral Cortex* 2013; **23**(12): 2944-55.

57. Ceschin R, Wisnowski JL, Paquette LB, Nelson MD, Blüml S, Panigrahy A. Developmental synergy between thalamic structure and interhemispheric connectivity in the visual system of preterm infants. *NeuroImage: Clinical* 2015.

58. Gertsvolf N, Votava-Smith JK, Ceschin R, et al. Association between Subcortical Morphology and Cerebral White Matter Energy Metabolism in Neonates with Congenital Heart Disease. *Scientific reports* 2018; **8**.

59. Harbison AL, Votava-Smith JK, Del Castillo S, et al. Clinical Factors Associated with Cerebral Metabolism in Term Neonates with Congenital Heart Disease. *The Journal of Pediatrics* 2017.

60. Paquette LB, Votava-Smith JK, Ceschin R, et al. Abnormal development of thalamic microstructure in premature neonates with congenital heart disease. *Pediatric cardiology* 2015; **36**(5): 960-9.

61. Schmithorst VJ, Votava‐Smith JK, Tran N, et al. Structural network topology correlates of microstructural brain dysmaturation in term infants with congenital heart disease. *Human brain mapping* 2018; **39**(11): 4593-610.

62. Wisnowski JL, Blüml S, Paquette L, et al. Altered glutamatergic metabolism associated with punctate white matter lesions in preterm infants. *Plos One* 2013; **8**(2): e56880.

63. Wisnowski JL, Schmithorst VJ, Rosser T, et al. Magnetic resonance spectroscopy markers of axons and astrogliosis in relation to specific features of white matter injury in preterm infants. *Neuroradiology* 2014: 1-9.

64. Paquette LB, Wisnowski JL, Ceschin R, et al. Abnormal cerebral microstructure in premature neonates with congenital heart disease. *AJNR American journal of neuroradiology* 2013; **34**: 2026-33.

65. Panigrahy A, Ceschin R, Lee V, et al. Respiratory Ciliary Motion Defect Predict Regional Brain Abnormalities and Increased Extra Axial CSF Fluid in Neonates With Complex Congenital Heart Disease. *Circulation* 2014; **130**(suppl_2): A16570-A.

66. Panigrahy A, Votava-Smith J, Lee V, et al. Abnormal Brain Connectivity and Poor Neurodevelopmental Outcome in Congenital Heart Disease Patients With Subtle Brain Dysplasia. *Circulation* 2015; **132**(suppl_3): A16541-A.

67. Votava-Smith JK, Tran N, Abbott J, et al. Impaired Cerebral Autoregulation is Associated With Brain Abnormalities in Neonatal Congenital Heart Disease: Initial Experience. *Circulation* 2016; **134**(suppl_1): A18081-A.

68. Lao Y, Wang Y, Shi J, et al. Thalamic alterations in preterm neonates and their relation to ventral striatum disturbances revealed by a combined shape and pose analysis. *Brain Structure and Function* 2014: 1-20.

69. Shi J, Wang Y, Ceschin R, et al. A multivariate surface-based analysis of the putamen in premature newborns: regional differences within the ventral striatum. *Plos One* 2013; **8**(7): e66736.

70. Serag A, Aljabar P, Ball G, et al. Construction of a consistent high-definition spatio-temporal atlas of the developing brain using adaptive kernel regression. *Neuroimage* 2012; **59**(3): 2255-65.

71. Votava-Smith JK, Gaesser J, Harbison AL, et al. Clinical Factors Associated with Microstructural Connectome Related Brain Dysmaturation in Term Neonates with Congenital Heart Disease. Cold Spring Harbor Laboratory; 2022.

72. Li Y, Klena NT, Gabriel GC, et al. Global genetic analysis in mice unveils central role for cilia in congenital heart disease. *Nature* 2015; **521**(7553): 520-4.

73. Damerla RR, Cui C, Gabriel GC, et al. Novel Jbts17 mutant mouse model of Joubert syndrome with cilia transition zone defects and cerebellar and other ciliopathy related anomalies. *Hum Mol Genet* 2015; **24**(14): 3994-4005.

74. Latal B, Patel P, Liamlahi R, Knirsch W, Tuura ROG, von Rhein M. Hippocampal volume reduction is associated with intellectual functions in adolescents with congenital heart disease. *Pediatric research* 2016; **80**(4): 531.

75. Fontes K, Rohlicek CV, Saint‐Martin C, et al. Hippocampal alterations and functional correlates in adolescents and young adults with congenital heart disease. *Human brain mapping* 2019.

76. Wu Y, Kapse K, Jacobs M, et al. Association of maternal psychological distress with in utero brain development in fetuses with congenital heart disease. *JAMA pediatrics* 2020; **174**(3): e195316-e.

77. BOLDUC ME, Limperopoulos C. Neurodevelopmental outcomes in children with cerebellar malformations: a systematic review. *Developmental Medicine & Child Neurology* 2009; **51**(4): 256-67.

78. Stoodley CJ. The cerebellum and neurodevelopmental disorders. *The Cerebellum* 2016; **15**(1): 34-7.

79. Zwicker JG, Miller SP, Grunau RE, et al. Smaller cerebellar growth and poorer neurodevelopmental outcomes in very preterm infants exposed to neonatal morphine. *The Journal of pediatrics* 2016; **172**: 81-7. e2.

80. Badaly D, Beers SR, Ceschin R, et al. Cerebellar and Prefrontal Structures Associated with Executive Functioning in Pediatric Patients with Congenital Heart Defects. *medRxiv* 2021.

81. Ramphal B, Whalen DJ, Kenley JK, et al. Brain connectivity and socioeconomic status at birth and externalizing symptoms at age 2 years. *Developmental cognitive neuroscience* 2020; **45**: 100811.

82. Graham AM, Buss C, Rasmussen JM, et al. Implications of newborn amygdala connectivity for fear and cognitive development at 6-months-of-age. *Developmental cognitive neuroscience* 2016; **18**: 12-25.

83. Taoudi-Benchekroun Y, Christiaens D, Grigorescu I, et al. Predicting age and clinical risk from the neonatal connectome. *NeuroImage* 2022; **257**: 119319.

84. Bhroin MN, Seada SA, Bonthrone AF, et al. Reduced structural connectivity in cortico-striatal-thalamic network in neonates with congenital heart disease. *NeuroImage: Clinical* 2020; **28**: 102423.

85. Haber SN. Corticostriatal circuitry. *Dialogues in clinical neuroscience* 2022.

86. Gordon EM, Laumann TO, Marek S, et al. Individualized functional subnetworks connect human striatum and frontal cortex. *Cerebral Cortex* 2022; **32**(13): 2868-84.

87. Giessel AJ, Datta SR. Olfactory maps, circuits and computations. *Current opinion in neurobiology* 2014; **24**: 120-32.

88. Millhouse OE, Heimer L. Cell configurations in the olfactory tubercle of the rat. *Journal of Comparative Neurology* 1984; **228**(4): 571-97.

89. Murata K, Kanno M, Ieki N, Mori K, Yamaguchi M. Mapping of learned odor-induced motivated behaviors in the mouse olfactory tubercle. *Journal of Neuroscience* 2015; **35**(29): 10581-99.

90. Fudge JL, Kunishio K, Walsh P, Richard C, Haber SN. Amygdaloid projections to ventromedial striatal subterritories in the primate. *Neuroscience* 2002; **110**(2): 257-75.

91. Russchen FT, Bakst I, Amaral DG, Price JL. The amygdalostriatal projections in the monkey. An anterograde tracing study. *Brain research* 1985; **329**(1-2): 241-57.

92. Kelley AE, Domesick VB, Nauta WJH. The amygdalostriatal projection in the rat—an anatomical study by anterograde and retrograde tracing methods. *Neuroscience* 1982; **7**(3): 615-30.

93. Krettek J, Price J. Amygdaloid projections to subcortical structures within the basal forebrain and brainstem in the rat and cat. *Journal of Comparative Neurology* 1978; **178**(2): 225-53.

94. Scott JW, McBride RL, Schneider SP. The organization of projections from the olfactory bulb to the piriform cortex and olfactory tubercle in the rat. *Journal of Comparative Neurology* 1980; **194**(3): 519-34.

95. Kosel KC, Van Hoesen GW, West JR. Olfactory bulb projections to the parahippocampal area of the rat. *Journal of Comparative Neurology* 1981; **198**(3): 467-82.

96. Zhang Z, Zhang H, Wen P, et al. Whole-brain mapping of the inputs and outputs of the medial part of the olfactory tubercle. *Frontiers in Neural Circuits* 2017; **11**: 52.

97. Leisman G, Braun-Benjamin O, Melillo R. Cognitive-motor interactions of the basal ganglia in development. *Frontiers in systems neuroscience* 2014; **8**: 16.

98. Ikemoto S. Dopamine reward circuitry: two projection systems from the ventral midbrain to the nucleus accumbens–olfactory tubercle complex. *Brain research reviews* 2007; **56**(1): 27-78.

99. Seubert J, Freiherr J, Frasnelli J, Hummel T, Lundström JN. Orbitofrontal cortex and olfactory bulb volume predict distinct aspects of olfactory performance in healthy subjects. *Cerebral Cortex* 2013; **23**(10): 2448-56.

100. De Smet HJ, Paquier P, Verhoeven J, Mariën P. The cerebellum: its role in language and related cognitive and affective functions. *Brain and language* 2013; **127**(3): 334-42.

101. Hoshi E, Tremblay L, Féger J, Carras PL, Strick PL. The cerebellum communicates with the basal ganglia. *Nature neuroscience* 2005; **8**(11): 1491-3.

102. Bostan AC, Dum RP, Strick PL. The basal ganglia communicate with the cerebellum. *Proceedings of the national academy of sciences* 2010; **107**(18): 8452-6.

103. O'Doherty JP, Dayan P, Friston K, Critchley H, Dolan RJ. Temporal difference models and reward-related learning in the human brain. *Neuron* 2003; **38**(2): 329-37.

104. Hikosaka O, Nakamura K, Sakai K, Nakahara H. Central mechanisms of motor skill learning. *Current opinion in neurobiology* 2002; **12**(2): 217-22.

105. Yagi H, Liu X, Gabriel GC, et al. The Genetic Landscape of Hypoplastic Left Heart Syndrome. *Pediatr Cardiol* 2018; **39**(6): 1069-81.

106. Tiana M, Acosta-Iborra B, Puente-Santamaria L, et al. The SIN3A histone deacetylase complex is required for a complete transcriptional response to hypoxia. *Nucleic Acids Res* 2018; **46**(1): 120-33.

107. Asahina H, Masuba A, Hirano S, Yuri K. Distribution of protocadherin 9 protein in the developing mouse nervous system. *Neuroscience* 2012; **225**: 88-104.

108. Wu Y, Jin X, Zhang Y, Zheng J, Yang R. Genetic and epigenetic mechanisms in the development of congenital heart diseases. *World J Pediatr Surg* 2021; **4**(2): e000196.

109. Bruneau BG. Signaling and transcriptional networks in heart development and regeneration. *Cold Spring Harb Perspect Biol* 2013; **5**(3): a008292.

110. Zhang QJ, Liu ZP. Histone methylations in heart development, congenital and adult heart diseases. *Epigenomics* 2015; **7**(2): 321-30.

111. Marino BS, Lipkin PH, Newburger JW, et al. Neurodevelopmental outcomes in children with congenital heart disease: evaluation and management: a scientific statement from the American Heart Association. *Circulation* 2012; **126**(9): 1143-72.

112. Newburger JW, Sleeper LA, Bellinger DC, et al. Early Developmental Outcome in Children With Hypoplastic Left Heart Syndrome and Related Anomalies. *Circulation* 2012; **125**(17): 2081-91.

113. Sananes R, Manlhiot C, Kelly E, et al. Neurodevelopmental outcomes after open heart operations before 3 months of age. *Ann Thorac Surg* 2012; **93**(5): 1577-83.

114. von Rhein M, Dimitropoulos A, Valsangiacomo Buechel ER, Landolt MA, Latal B. Risk factors for neurodevelopmental impairments in school-age children after cardiac surgery with full-flow cardiopulmonary bypass. *J Thorac Cardiovasc Surg* 2012; **144**(3): 577-83.

115. Naef N, Liamlahi R, Beck I, et al. Neurodevelopmental Profiles of Children with Congenital Heart Disease at School Age. *J Pediatr* 2017; **188**: 75-81.

116. Verrall CE, Blue GM, Loughran-Fowlds A, et al. 'Big issues' in neurodevelopment for children and adults with congenital heart disease. *Open Heart* 2019; **6**(2): e000998.

117. Sood E, Jacobs JP, Marino BS. Optimising neurodevelopmental and psychosocial outcomes for survivors with CHD: a research agenda for the next decade. *Cardiol Young* 2021; **31**(6): 873-5.

118. Jacobsen RM. Outcomes in Adult Congenital Heart Disease: Neurocognitive Issues and Transition of Care. *Pediatr Clin North Am* 2020; **67**(5): 963-71.

119. Marelli A, Miller SP, Marino BS, Jefferson AL, Newburger JW. Brain in Congenital Heart Disease Across the Lifespan: The Cumulative Burden of Injury. *Circulation* 2016; **133**(20): 1951-62.

120. Bellinger DC, Wypij D, Rivkin MJ, et al. Adolescents with d-transposition of the great arteries corrected with the arterial switch procedure: neuropsychological assessment and structural brain imaging. *Circulation* 2011; **124**(12): 1361-9.

121. Schaefer C, von Rhein M, Knirsch W, et al. Neurodevelopmental outcome, psychological adjustment, and quality of life in adolescents with congenital heart disease. *Dev Med Child Neurol* 2013; **55**(12): 1143-9.

122. Fahed AC, Gelb BD, Seidman JG, Seidman CE. Genetics of Congenital Heart Disease. *Circulation Research* 2013; **112**(4): 707-20.

123. Zaidi S, Brueckner M. Genetics and Genomics of Congenital Heart Disease. *Circulation Research* 2017; **120**(6): 923-40.

124. Jenkins KJ, Correa A, Feinstein JA, et al. Noninherited Risk Factors and Congenital Cardiovascular Defects: Current Knowledge. *Circulation* 2007; **115**(23): 2995-3014.

125. Zaidi S, Choi M, Wakimoto H, et al. De novo mutations in histone-modifying genes in congenital heart disease. *Nature* 2013; **498**(7453): 220-3.

126. Cassidy AR, Butler SC, Briend J, et al. Neurodevelopmental and psychosocial interventions for individuals with CHD: a research agenda and recommendations from the Cardiac Neurodevelopmental Outcome Collaborative. *Cardiol Young* 2021; **31**(6): 888-99.

Figure and Figure Legends

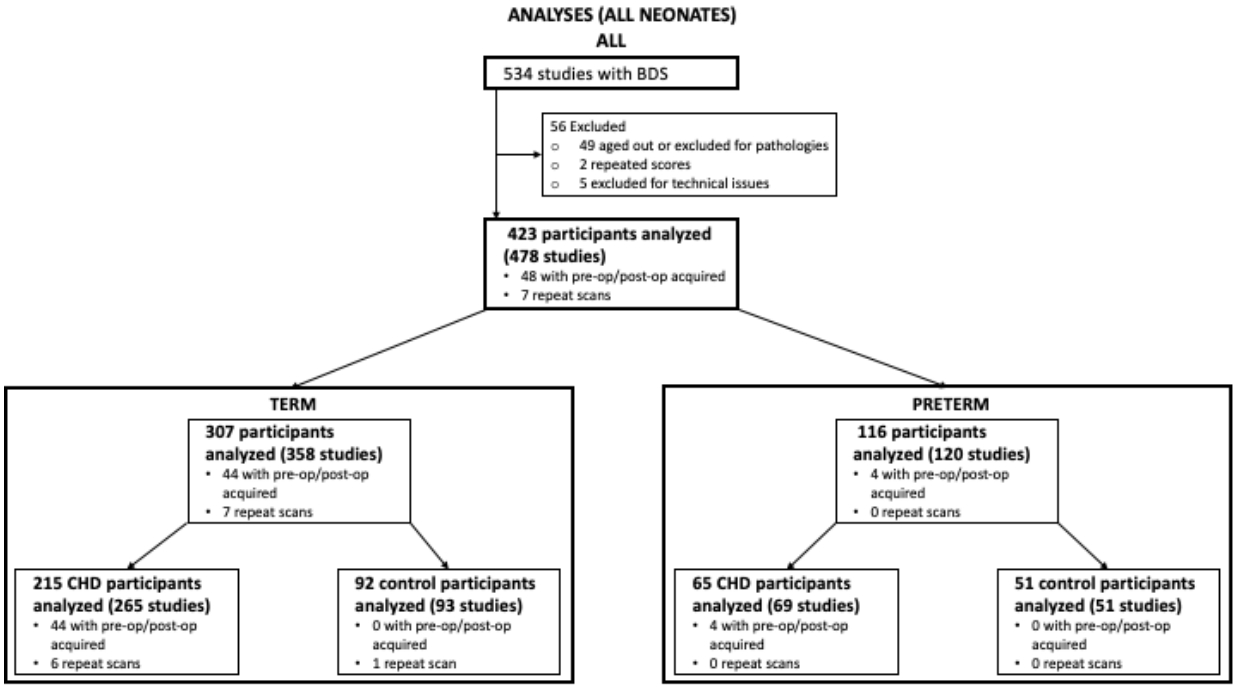

Figure 1. Recruitment Flowchart and Subject Numbers. Study initially consisted of 534 subjects which were scored using the brain dysplasia score (BDS). Initial subjects consisted of 307 term and 116 pre-term individuals.

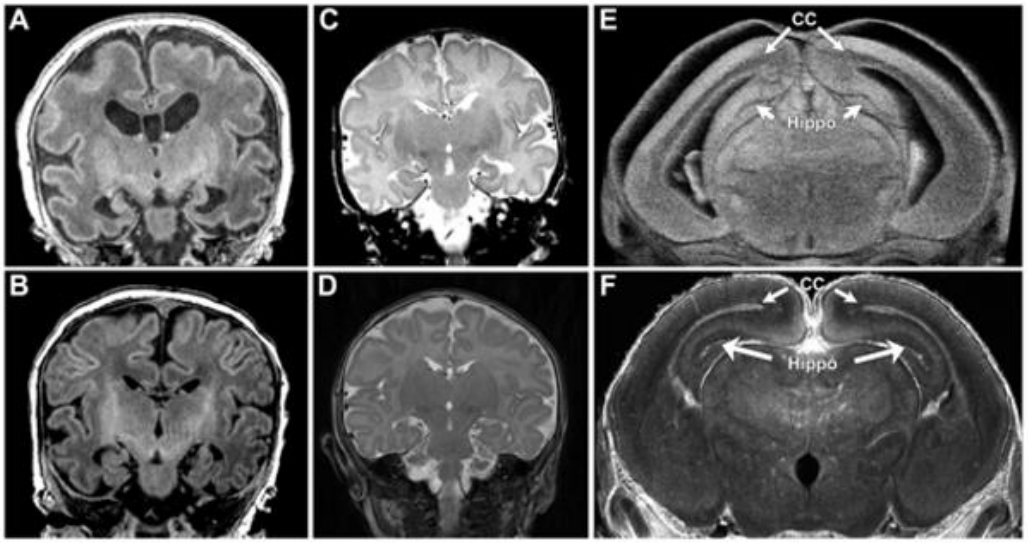

Figure 2. Hippocampal Abnormalities Were Similar Among Human and Mouse. Panel (a)(b)(c)and (d) demonstrate abnormal hypoplastic and/or malrotated hippocampi in infants with CHD which comparable abnormalities noted in the mouse mutant (e). A mouse control is shown for comparison in (f) depicts an abnormal. Panel (b)

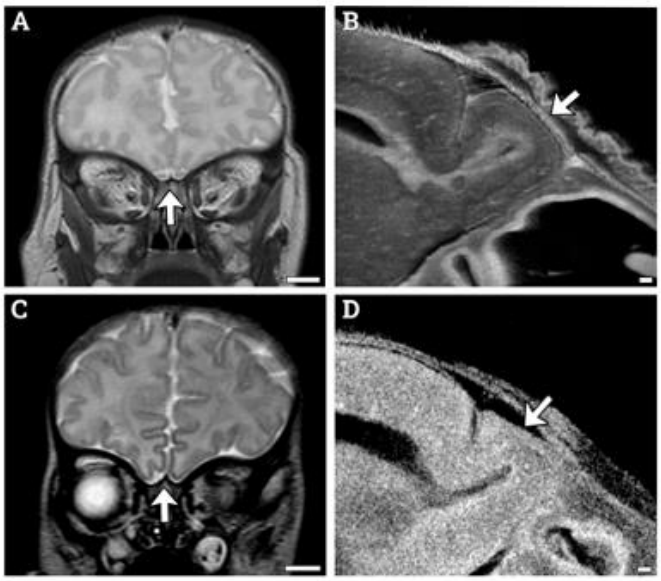

Figure 3. Consistent Olfactory Bulb Phenotype is Visible Among Human and Mouse. (a) Human control subject exhibits normal olfactory bulb size and structure. (b) Mouse control showing olfactory bulb with normal shape and size. (c) HLHS human subject with aplastic olfactory bulbs. (d) Mouse with Congenital heart disease with hypoplastic olfactory bulb.

1098

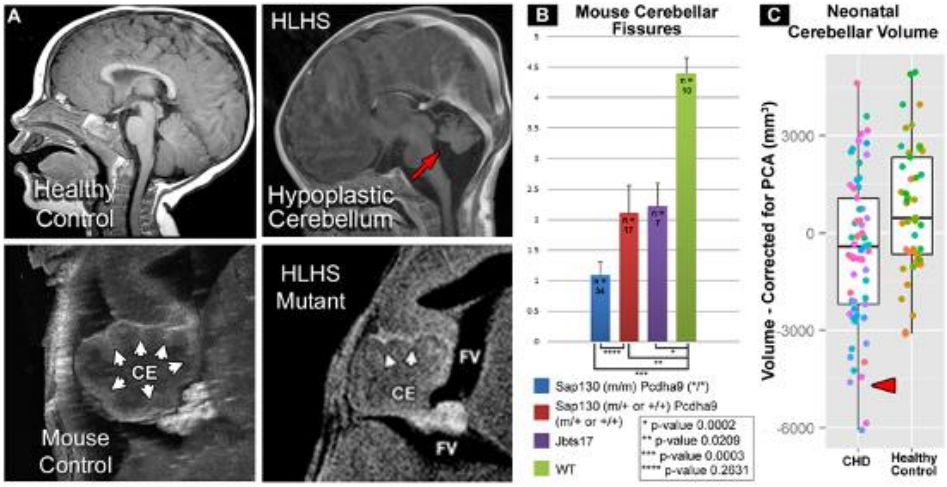

1099

1100 **Figure 4. Cerebellar Abnormalities Seen in Both Human and Mouse.** Panels (a) and (b) depict a human subject
1101 with HLHS compared to a healthy control. The cerebellum of the HLHS subject is hypoplastic shows
1102 dysmaturation. Panels (c) and (d) show a mouse with HLHS and a normal control. The cerebellum of the HLHS
1103 mutant displayed hypoplasia and a lesser number of cerebellar fissures. (e) Average number of cerebellar fissures
1104 among mouse groupings. (f) Human neonatal cerebellar residual volumes with gestational age regressed out.

1105

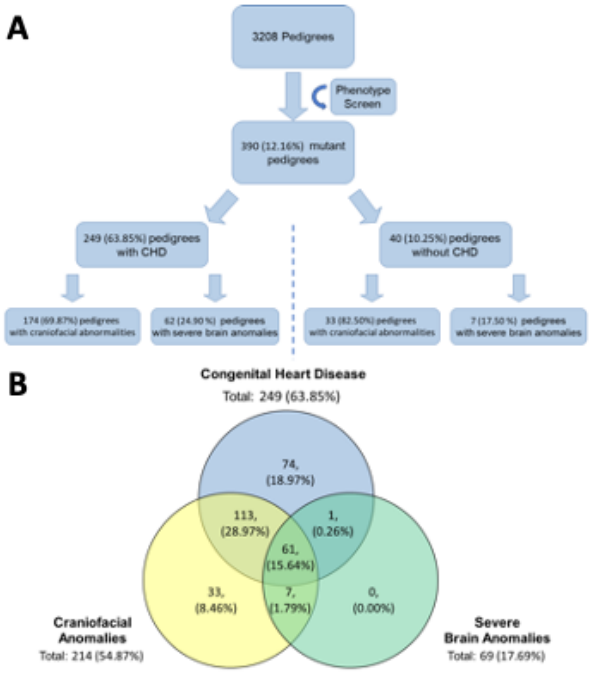

Figure 5. Phenotype Mouse Screen Recovered Mutant Mice with Defects in Cardiac, Brain and Craniofacial. (a) From the original phenotype screen 390 mutant lines were identified. Of those 390 lines 249 had CHD and of those, 174 and 62 had craniofacial and severe brain anomalies, respectively. Of the 40 lines that didn't have CHD, 33 had craniofacial and 7 had severe brain anomalies. (b) Three major groupings, congenital heart disease, craniofacial anomalies, and server brain anomalies, identified from the original phenotype screen and their relationship to one another. The highest overlap between two conditions is congenital heart disease and craniofacial anomalies at approximately 29% of the original 390 mutants identified.

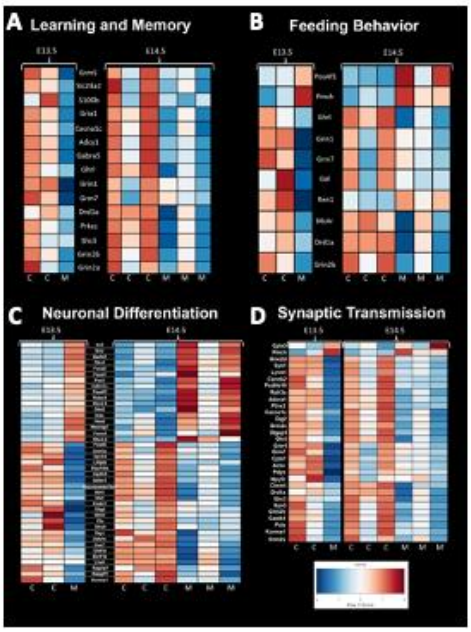

Figure 6. Mouse RNA Sequencing Analysis Shows Significant Difference in Gene Expression. (a) Genes associated with learning and memory showed lesser expression in control mice compared to Ohia mutant mice. (b) Genes associated with feeding behavior showed an abnormal pattern in Ohia mice. Ohia mice showed a pattern of expression that was opposite compared control mice at both time points. (c) Genes associated with neuronal differentiation showed a opposite pattern of expression in Ohia mutant mice compared to controls. (d) Genes associated with synaptic transmission had a different expression pattern in Ohia mutant mice compared to controls.

1123 **Supplemental Figure Legends**

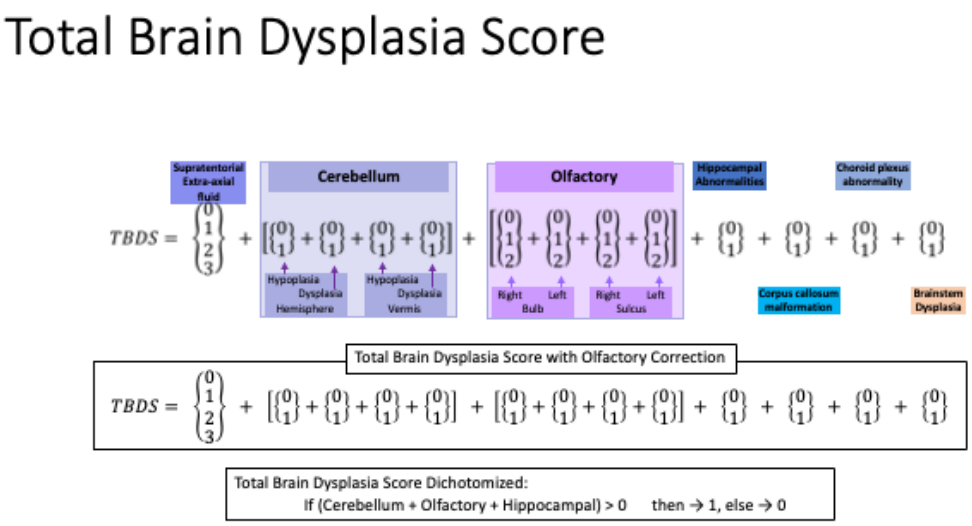

1124

1125 **Supplemental Figure 1. Components of Human Brain Dysplasia Scoring Criteria.** Our brain dysplasia scoring
1126 criteria consisted of 13 distinct observations. Supratentorial extra-axial fluid was assessed for normality, cerebellar
1127 hemisphere and vermis were assessed for hypoplasia and dysplasia, right and left olfactory bulb and olfactory
1128 sulcus were examined for any abnormalities. Additionally, the hippocampus, corpus collosum, choroid plexus, and
1129 brainstem were checked for abnormalities.

1130

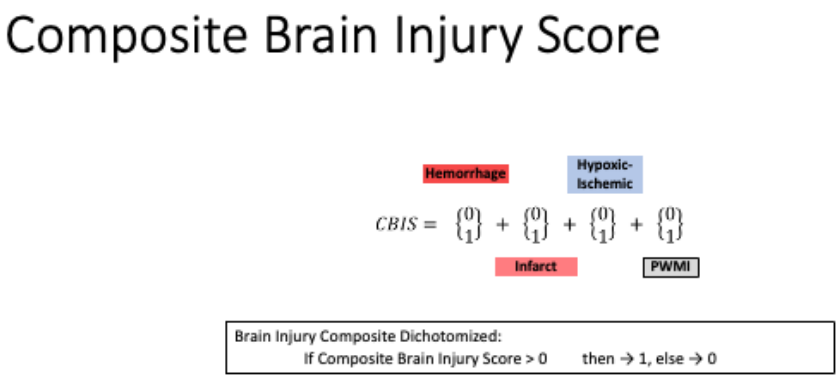

Supplemental Figure 2. Components of Composite Brain Injury Score. Brain injury score was composed of four measures: hemorrhage, infarct, hypoxic ischemia, and perinatal white matter injury. Brain injury score was binary, if any injury was present in the above measures, the subject was considered to have a brain injury.

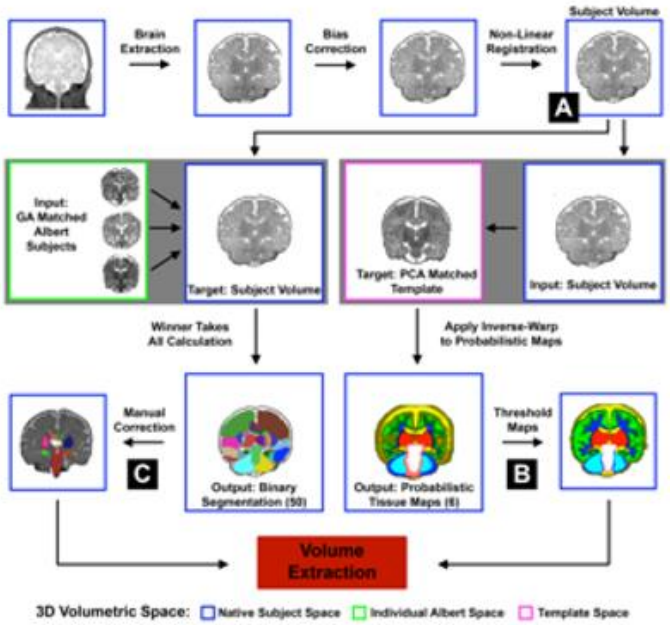

Supplemental Figure 3. Flow Diagram for NeBSS, a Semi-automated Neonatal Segmentation Pipeline. Briefly, subject MR images are input into NeBSS which has two branches. Branch A uses the Albert Neonatal Atlas and outputs 50 distinct volumetric brain structures in the subject space. Branch B uses the Serag Neonatal Brain Atlas probability maps to output 10 volumetric brain regions.

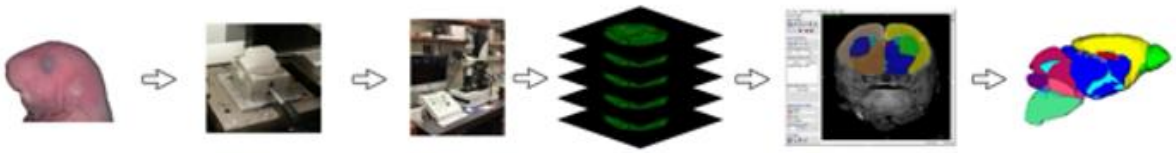

Supplemental Figure 4. Flow Diagram of Sample Preparation, ECM Analysis, and Volumetric Analysis. Samples selected for analysis were first necropsied. Post-necropsy samples were dehydrated using a Sakura Tissue Tek system and processed on the ECM machine. Samples were then manually segmented using ITK-Snap before volumetric results were analyzed.

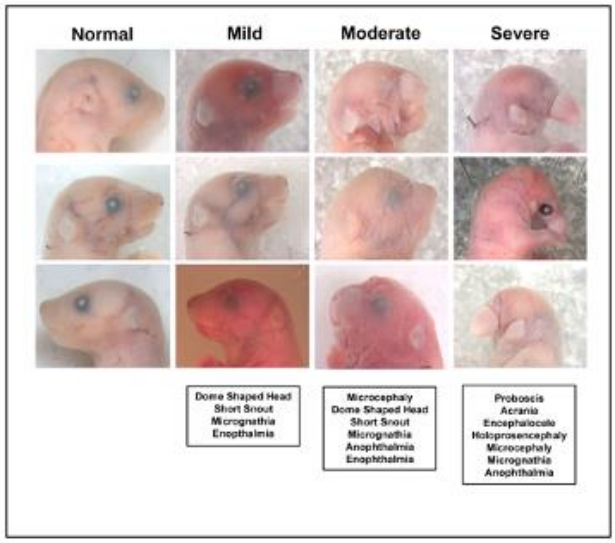

Supplemental Figure 5. Necropsy Among Mutant Mice Showed Variety and Differing Degree of Severity of Malformations. Mice in the mouse screen presented with craniofacial anomalies with varying degrees of severity. More mild forms of errant craniofacial anatomy presented with mild defects in the ears and eyes. Moderate forms presented as more severe ear and eye defects as well as a shortened snout. Lastly, severe defects presented with large structural defects in the craniofacial anatomy, often with underlying structural brain defects as well.

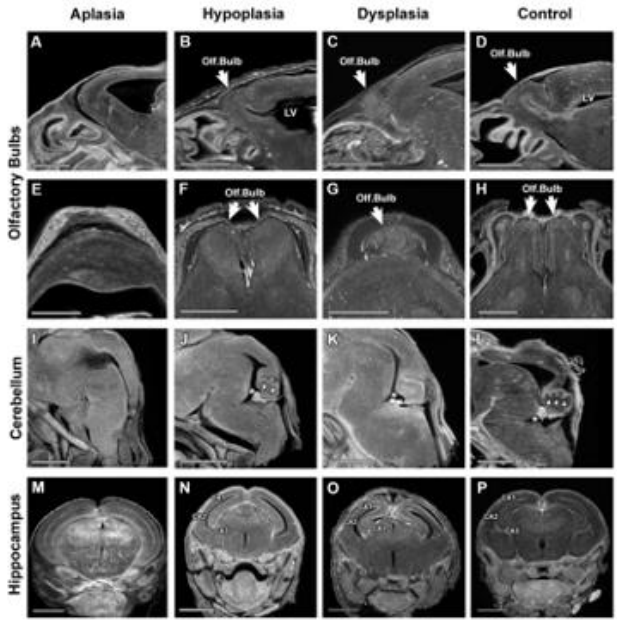

Supplemental Figure 6. Individual Structures Showed a Range of Abnormality in Screen Mice. Episcopic Fluorescence Image Capture (ECM) was carried out on prepared mouse brains. Samples presented with varying degrees of abnormalities. Three major structures analyzed were olfactory bulbs, cerebellum, and hippocampus. Within each structure, mice had a variety of defects including aplasia, hypoplasia, and dysplasia.

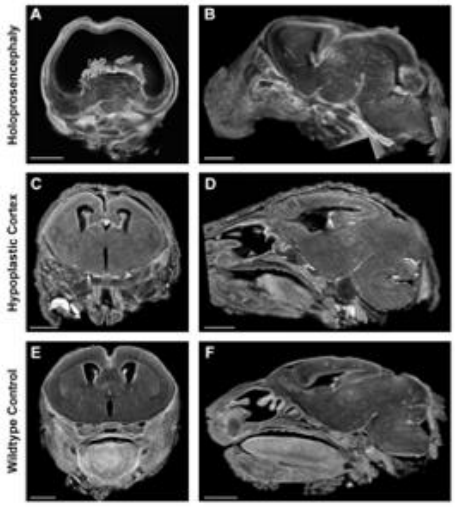

Supplemental Figure 7. Varying Degree of Cerebral Abnormalities Present in Screen Mice. ECM analysis found that mice had varying degrees of severity of cerebral abnormalities including holoprosencephaly and cerebral hypoplasia.

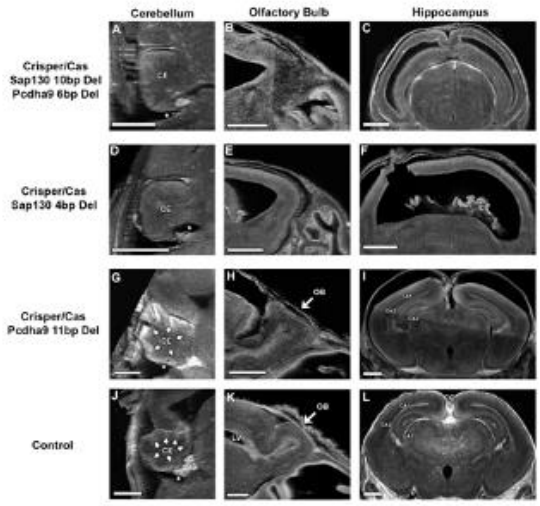

1166

1167 **Supplemental Figure 8. Crispr/Cas Figure Mutant Animals Showed Similar Phenotype to Screen Mice.**
1168 Using ECM, Crispr/Cas9 mutants were analyzed and show similar phenotypes seen in mutant mice recovered from
1169 the phenotype screen. A similar pattern of dysplasia and aplasia were seen in the cerebellum, olfactory bulb and
1170 hippocampus of mice recovered in the screen.

1171

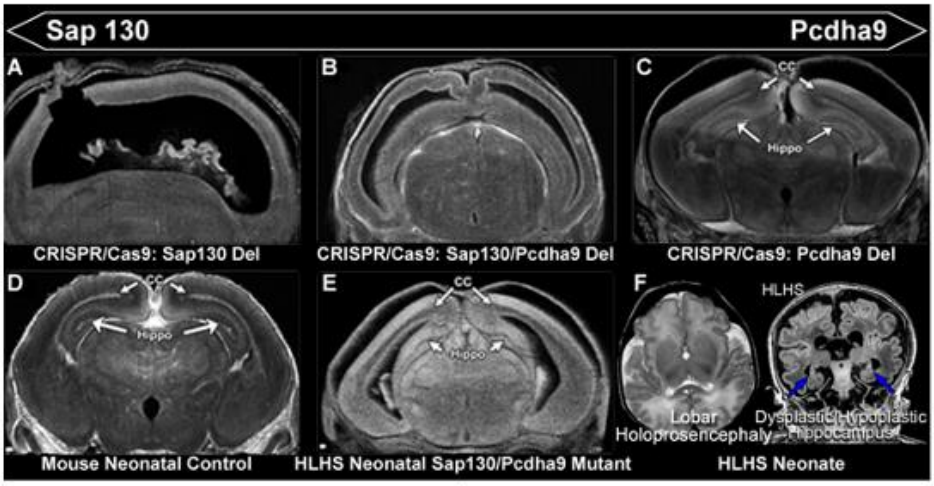

Supplemental Figure 9. Holoprosencephaly and Hippocampal Malformations Seen in Human and Mouse. A, Alobar holoprosencephaly seen in Sap130 CRISPR/Cas9 deletion mouse. B, Lobar holoprosencephaly seen in Sap130/Pcdha9 double CRISPR/Cas9 deletion mouse. C, Pcdha9 CRISPR/Cas9 deletion mouse displaying cerebral hypoplasia and dysmaturation as well as hippocampal abnormalities. D, Control mouse showing normal cortical and hippocampal anatomy. E, Sap130/Pcdha9 double mutant mouse exhibiting cortical, corpus collosum, and hippocampal abnormalities. F, Lobar holoprosencephaly and hippocampal malformations observed in human subjects with HLHS.

Table 1: Incidence of Subcortical Brain Dysmaturation in Preterm/Term CHD And Controls

BDS Abnormalities (Dichotomous)	**Preterm CHD (*n* = 69)**	**Preterm Non-CHD (*n* = 51)**	**Comparison**	**Term CHD (*n* = 263)**	**Term Control (*n* = 93)**	**Comparison**
	Number of Subjects with Abnormality *(%)*		**p-value**	**Number of Subjects with Abnormality *(%)***		**p-value**
Bilateral Cerebellar Hemispheric Hypoplasia	13 (18.84%)	1 (1.96%)	**0.0049**	30 (11.41%)	0 (0.00%)	**0.0006**
Bilateral Cerebellar Hemispheric Dysplasia	7 (10.14%)	1 (1.96%)	0.0607	15 (5.70%)	0 (0.00%)	**0.0133**
Cerebellar Vermis Hypoplasia	18 (26.09%)	3 (5.88%)	**0.0040**	58 (22.05%)	0 (0.00%)	**<0.0001**
Cerebellar Vermis Dysplasia	9 (13.04%)	0 (0.00%)	**0.0049**	23 (8.75%)	0 (0.00%)	**0.0019**
Dichotomized Cerebellar Composite	26 (37.68%)	3 (5.88%)	**<0.0001**	75 (28.52%)	0 (0.00%)	**<0.0001**
Right Olfactory Bulb	24 (34.78%)	4 (7.84%)	**<0.0001**	127 (48.29%)	8 (8.60%)	**<0.0001**
Left Olfactory Bulb	25 (36.23%)	4 (7.84%)	**<0.0001**	126 (47.91%)	9 (9.68%)	**<0.0001**
Right Olfactory Sulcus	23 (33.33%)	1 (1.96%)	**<0.0001**	109 (41.44%)	3 (3.23%)	**<0.0001**
Left Olfactory Sulcus	23 (33.33%)	1 (1.96%)	**<0.0001**	109 (41.44%)	2 (2.15%)	**<0.0001**
Dichotomized Olfactory Composite	28 (40.58%)	4 (7.84%)	**<0.0001**	127 (48.29%)	9 (9.68%)	**<0.0001**
Hippocampus	34 (49.28%)	11 (21.57%)	**0.0019**	117 (44.49%)	3 (3.23%)	**<0.0001**
Corpus Callosum	10 (14.49%)	0 (0.00%)	**0.0045**	26 (9.89%)	0 (0.00%)	**0.0016**
Choroid Plexus	30 (43.48%)	3 (5.88%)	**<0.0001**	108 (41.06%)	8 (8.60%)	**<0.0001**
Brainstem	10 (14.49%)	0 (0.00%)	**0.0045**	25 (9.51%)	0 (0.00%)	**0.0020**
BDS Abnormalities (Categorical)	**Mean *(Standard Error)***		**p-value**	**Mean *(Standard Error)***		**p-value**
Supratentorial Extra-Axial Fluid*	0.9839 *(0.0989)*	0.6000 *(0.1069)*	**0.0075**	0.8071 *(0.0495)*	0.3516 *(0.0527)*	**<0.0001**
Cerebellar Composite	0.6812 *(0.1121)*	0.0980 *(0.0578)*	**<0.0001**	0.4791 *(0.0536)*	0.0000 *(0.0000)*	**<0.0001**
Olfactory Composite	1.6912 *(0.2693)*	0.1961 *(0.1011)*	**<0.0001**	2.0229 *(0.1452)*	0.2418 *(0.0817)*	**<0.0001**
Subcortical BDS Composite	4.3188 *(0.4043)*	1.1569 *(0.2046)*	**<0.0001**	4.1141 *(0.2210)*	0.6989 *(0.1268)*	**<0.0001**

Table 2A: Correlation of Brain Dysplasia Score (BDS) with Demographic Factors (Entire cohort:Univariate Analysis)

Dependent	Independent	N-used	R-Square	p-value	estimate
BDS	Sex	490	0.000026	0.9096	-0.0359
BDS	GA	487	0.003619	0.1851	0.058461
BDS	PCA	489	0.001664	0.368	0.011933

Table 2B: Correlation of Brain Dysplasia Score (BDS) with Demographic Factors (CHD cohort, Univariate Analysis)

Dependent	Independent	N-used	R-Square	p-value	estimate
BDS	Sex	344	0.008447	0.0887	0.680037
BDS	Genetic Abnormality	252	0.045926	**0.0006**	-1.66277
BDS	GA	341	0.00002	0.9352	-0.00562
BDS	PCA	343	0.002649	0.3419	0.017322
BDS	Birth Weight	248	0.000337	0.7737	-9.1E-05
BDS	Pre/Post operative status	343	0.000662	0.6349	-0.18132
BDS	Term/Preterm	343	0.000651	0.6378	-0.23214

Table 2C: Correlation of Brain Dysplasia Score (BDS) with Demographic Factors in (CHD cohort, Multivariate Analysis)

			Independent		Term/Preterm		Pre/Post	
Dependent	N-used	R-Square	p-value	estimate	p-value	estimate	p-value	estimate
Sex	343	0.009957	0.0854	0.6942	0.7409	-0.1633	0.5872	-0.2074
Genetic Abnormality	252	0.048769	**0.0006**	-1.6806	0.3971	-0.4741	0.8911	-0.0617
GA	341	0.002196	0.6323	0.059	0.5401	-0.5386	0.5487	-0.2303
PCA	343	0.003471	0.3867	0.0168	0.6152	-0.2489	0.8939	-0.0543
Birth Weight	248	0.027317	0.4891	0.0002	0.0368	-1.4958	0.0878	-0.7169

Table 3: Correlation of Brain Dysplasia Score, Brain Injury and Cortical Maturation Score (TMS)

				Main Independent Factor		PCA	
	N-used	model p	R-Square	p-value	estimate	p-value	estimate
Hemorrhage	340	0.9876	0.000001	0.9876	0.010146	—	—
Infarction	341	0.604	0.000794	0.604	0.345161	—	—
Hypoxic ischemic injury	328	0.6111	0.000794	0.6111	-0.55119	—	—
Punctate white matter lesion	342	0.8922	0.000054	0.8922	0.071424	—	—
Any brain injury, dichotomized	344	0.5548	0.001021	0.5548	0.243539	—	—
Brain injury composite score	344	0.9042	0.000042	0.9042	-0.03758	—	—
Maturation, Cortical Fold	332	**0.0016**	0.029645	0.0016	-0.7302	—	—
Maturation, Frontal Cortex	332	**<0.0001**	0.061511	<0.0001	-0.80238	—	—
Maturation, Insular Cortex	332	**<0.0001**	0.067464	<0.0001	-1.01932	—	—
Maturation, Cortical Fold & PCA	331	**0.0044**	0.032554	0.001	-0.78513	0.3255	0.02414
Maturation, Frontal Cortex & PCA	331	**<0.0001**	0.067676	<0.0001	-0.86858	0.1531	0.034607
Maturation, Insular Cortex & PCA	331	**<0.0001**	0.07442	<0.0001	-1.10484	0.146	0.035021

Table 4: Association Between Brain Dysplasia Score and Term Infant Regional Brain Volumes by CHD Status

Normalized Volumes (n = 105)	Correlation with BDS (term CHD and term control cohort combined)	Comparison between term CHD and term control cohorts
	p-value *(correlation)*	**p-value *(direction)***
Right Hippocampus	0.0749 *(N.S.)*	0.1476 *(N.S.)*
Left Hippocampus	0.1329 *(N.S.)*	0.3784 *(N.S.)*
Right Cerebellum	0.0535 *(N.S.)*	0.1476 *(N.S.)*
Left Cerebellum	**0.0433 *(-)***	0.1887 *(N.S.)*
Cerebellum	**0.0299 *(-)***	**0.0087 *(CHD > CON)***
Cerebrospinal Fluid (CSF)	0.0517 *(N.S.)*	**0.0026 *(CHD > CON)***
Infratentorial CSF	0.2259 *(N.S.)*	0.9300 *(N.S.)*
Intraventricular CSF	**<0.0001 *(+)***	0.7398 *(N.S.)*
Supratentorial CSF	**0.0008 *(+)***	0.3535 *(N.S.)*
Deep Grey Matter	**0.0138 *(-)***	0.4877 *(N.S.)*
White Matter	0.4550 *(N.S.)*	0.6066 *(N.S.)*
Cerebral Cortex	0.1687 *(N.S.)*	**0.0016 *(CHD > CON)***
Brainstem	**0.0391 *(-)***	0.1311 *(N.S.)*

Table 5: Correlation between Brain Dysplasia Score and Clinical Feeding Outcomes

BDS Abnormalities (Clinical Outcome Correlates)	Lack of PO Feeds Prior to Discharge p-value	Length of Hospitalization p-value
Hippocampus	**0.0025**	**0.0090**
Right / Left Olfactory Bulbs	**0.0090 / 0.0050**	**0.0400 / 0.0300**
Right / Left Olfactory Sulci	**0.0070 / 0.0070**	**0.0700 / 0.0700**
Extra-Axial Fluid	**0.0030**	**<0.0001**
Bilateral Cerebellar Hemispheres	**0.0037**	**<0.0001**
Cerebellar Vermis	**0.0001**	**0.0002**
Brainstem	**<0.0001**	**N.S.**
Corpus Callosum	**0.0010**	**0.0100**
Choroid Plexus	**0.0100**	**0.0020**
Total Composite	**0.0001**	**0.0020**

Table 6 : Correlation between Brain Dysplasia Score and 15-18 Month Neurodevelopmental Outcomes

Neurodevelopmental Outcomes (n=90) (Total BDS Correlates)	**Non-Parametric**			**Parametric**
	Wilcoxon Mann-Whitney p-value (normal approx.)	**Wilcoxon Mann-Whitney p-value (T approx.)**	**Kruskal-Wallis p-value ($\chi 2$)**	**T-Test p-value**
Expressive Language Below Mean	**0.0160**	**0.0190**	**0.0160**	**0.0047**
Language Composite Below Mean	0.2810	0.2840	0.2790	0.2837
Language Delay	**0.0380**	**0.0420**	**0.0370**	**0.0181**
Developmental Delay (delayed in $\geq$ 1 domains)	**0.0280**	**0.0303**	**0.0272**	**0.0284**
Global Developmental Delay (delayed in $\geq$ 2 domains)	0.1070	0.1110	0.1060	0.1005

Table 7: Incidence of Brain Dysplasia Score and Subcomponents between Ohia and Wild type Mouse Mutants

Structure	Ohia Average	Wild Type Average	P value †
BDS Total	**4.42**	0	**<0.001**
Cerebellar Fissures	**1.5**	4.4	**<0.001**
	Ohia Incidence	**Wild Type Incidence**	**P value ***
BDS Dichotomized	**55/69, (79.71%)**	0/10, (0.00%)	**<0.001**
BDS Hippocampus or Cerebellum	**58/69, (84.06%)**	0/10, (0.00%)	**<0.001**
Aplastic Hippocampus	8/69, (11.59%)	0/10, (0.00%)	0.384
Hypoplastic Hippocampus	14/68, (20.59%)	0/10, (0.00%)	0.223
Dysplastic Hippocampus	**44/68, (64.71%)**	0/10, (0.00%)	**0.002**
Combination Hippocampus	22/69, (31.88%)	0/10, (0.00%)	0.133
Hypoplastic Cerebrum	13/68, (19.12%)	0/10, (0.00%)	0.244
Dysplastic Cerebrum	**43/68, (63.24%)**	0/10, (0.00%)	**0.003**
Aplastic Cerebellum	2/69, (02.90%)	0/10, (0.00%)	0.678
Hypoplastic Cerebellum	9/67, (13.43%)	0/10, (0.00%)	0.345
Dysplastic Cerebellum	**49/67, (73.13%)**	0/10, (0.00%)	**<0.001**
Combination Cerebellum	11/69, (15.94%)	0/10, (0.00%)	0.325
Aplastic Left Olfactory Bulb	**33/69, (47.83%)**	0/10, (0.00%)	**0.024**
Aplastic Right Olfactory Bulb	**34/69, (49.28%)**	0/10, (0.00%)	**0.02**
Hypoplastic Left Olfactory Bulb	9/67, (13.43%)	0/10, (0.00%)	0.345
Hypoplastic Right Olfactory Bulb	7/65, (10.77%)	0/10, (0.00%)	0.404
Dysplastic Left Olfactory Bulb	2/67, (2.99%)	0/10, (0.00%)	0.673
Dysplastic Right Olfactory Bulb	0/65, (00.00%)	0/10, (0.00%)	—
Combination Left Olfactory Bulb	**42/69, (60.87%)**	0/10, (0.00%)	**0.006**
Combination Right Olfactory Bulb	**41/69, (59.42%)**	0/10, (0.00%)	**0.007**
Hypoplastic Brainstem	0/66, (00.00%)	0/10, (0.00%)	—
Dysplastic Brainstem	20/67, (29.85%)	0/10, (0.00%)	0.12
Hypoplastic Midbrain	0/67, (00.00%)	0/10, (0.00%)	—
Dysplastic Midbrain	18/67, (26.87%)	0/10, (0.00%)	0.148

† Student's T-test was used to compare Cerebellar Fissure count and BDS Total Score. Chi-square analysis was used to compare individual structures as well as BDS Dichotomized and BDS Hippocampus or Cerebellum.*

Table 8: Relationship between Brain Dysplasia Scores/Cerebellar Fissures and Cardiac Lesion Subtypes in Ohia CHD/HLHS Preclinical Groups

	CHD vs. No CHD			Single vs. Biventricular Morphology			Conotruncal vs. Non Conotruncal			Cyanotic vs. Acyanotic			Arch Obstruction vs. No Obstruction		
	CHD	No CHD	P value *	Single	Double	P value *	Conotruncal	Non Conotruncal	P value *	Cyanotic	Acyanotic	P value *	Obstruction	No Obstruction	P value *
Cerebellar Fissures	1.17 ± 1.55	3.14 ± 1.67	**<0.001**	1.50 ± 2.12	1.16 ± 1.55	0.86	1.13 ± 1.92	1.22 ± 1.36	0.88	1.16 ± 1.80	1.19 ± 1.39	0.96	0.81 ± 0.98	1.48 ± 1.87	0.13
BDS Total	5.43 ± 2.22	2.73 ± 2.46	**<0.001**	7.00 ± 2.00	5.32 ± 2.20	0.21	5.27 ± 2.12	5.33 ± 2.46	0.93	5.63 ± 2.34	5.29 ± 2.17	0.61	5.87 ± 1.69	5.00 ± 2.60	0.12

** Student T-test used to calculate difference between population values within cerebellar fissures and Total Brain Dysmaturation Score (BDS).*

Table 9: Relationship of Genotype to Incidence of Subcortical Abnormalities used to Derive BDS score in CHD/HLHS Preclinical Groups

Group	A†	B‡	C§	D‖	E¶	F#
N Total	24	8	7	4	0	20
Olfactory bulb abnormality	18 (75%)	6 (75%)	6 (85.7%)	4 (100%)	0	9 (45%)
Cerebellar abnormality	21 (87.5%)	7 (87.5%)	7 (100%)	4 (100%)	0	13 (65%)
Hippocampus abnormality	21 (87.5%)	7 (87.5%)	6 (85.7%)	4 (100%)	0	13 (65%)
Brainstem abnormality	10 (42%)	2 (25%)	0 (0%)	2 (50%)	0	6 (30%)

†Group A: N 24, Genotype: Pcdha9(m/m) Sap130(m/m)

‡ Group B: N 8, Genotype: Pcdha9(m/+) Sap130(m/m)

§ Group C: N 7, Genotype: Pcdha9(+/+) Sap130(m/m)

‖ Group D: N 4, Genotype: Pcdha9(m/m) Sap130(m/+)

¶ Group E: N 0, Genotype: Pcdha9(m/m) Sap130(+/+)

Group F: N 27, Genotype: Pcdha9(m/+) or (+/+) Sap130(m/+) or (+/+)

Table 10: Relationship of Genotype to BDS Score in CHD/HLHS Preclinical Groups

	ABC vs. WT‡‡**			**ABC** vs. F#**			**AB†† vs. F#**			**A† vs. C§**			**B‡ vs. D‖**		
Structure	ABC Median	WT Median	P value*	ABC Median	F Median	P value *	AB Median	F Median	P value *	A Median	C Median	P value *	B Median	D Median	P value *
BDS Hippocampus or Cerebellum	1	0	**<0.001**	1	1	**0.008**	1	1	**0.021**	1	1	0.583	1	1	0.46
BDS Total	6	0	**<0.001**	6	5.5	0.227	6	5.5	0.251	6	5	0.56	6	6.5	0.558

** Non-parametric Mann–Whitney U test used to analyze differences in continuous Brain Dysmaturation Score.*

†Group A: N 24, Genotype: Pcdha9(m/m) Sap130(m/m)

‡ Group B: N 8, Genotype: Pcdha9(m/+) Sap130(m/m)

§ Group C: N 7, Genotype: Pcdha9(+/+) Sap130(m/m)

‖ Group D: N 4, Genotype: Pcdha9(m/m) Sap130(m/+)

¶ Group E: N 0, Genotype: Pcdha9(m/m) Sap130(+/+)

Group F: N 27, Genotype: Pcdha9(m/+) or (+/+) Sap130(m/+) or (+/+)

** Group ABC: N 39, Genotype: Sap130(m/m), Pcdha9 (*/*)

†† Group AB: N 32, Genotype: Sap130(m/m), Pcdha9 (m/*)

‡‡ Group WT: N 10